Journal of Chemical&Engineering Data

pubs.acs.org/jced Article

Round Robin Measurements of Molten Salt Properties for LiF-NaF-KF (FLiNaK) and NaCl-KCl Mixtures

Troy Munro, Randall Chiu, Melissa A. Rose, Ondrej Benes, Miroslav Boca, D. Nathanael Gardner, Amanda Leong, Sara Mastromarino, Kim L. Pamplin, Markus H. A. Piro, Mouna Saoudi, Juliano Schorne-Pinto, Christian Michael Sclafani, Anna L. Smith, Nathan D. Smith, Dino Sulejmanovic, Allison M. Berry, Renkun Chen, Ka Man Chung, Christa Dahman, Kent Detrick, Tianshi Feng, J. A. Ocádiz Flores, Ryan Gallagher, Levi Gardner, Xiaofeng Guo, J. Matthew Jackson, Toni Karlsson, Peter Kasper, Hojong Kim, Logan McIlwain, Matthew Memmott, Brian Merritt, Marisa J. Monreal, Kentaro Oishi, Liana Orlovskaya, S. Scott Parker, Andrew A. Prudil, Aaron D. Robison, Sean Scott, Raul C. Romero, III, John Vlieland, Michael E. Woods, Jinsuo Zhang, Theodore M. Besmann, and Raluca O. Scarlat*

Cite This: https://doi.org/10.1021/acs.jced.5c00421 Read Online

ACCESS | Metrics & More | Article Recommendations | Supporting Information

ABSTRACT: The development, operation, and regulation of nuclear reactors that utilize molten salts as fuel or as heat transfer media require knowledge of the thermal properties of the salt systems and quantification of the corresponding uncertainties. Knowledge of molten salt properties is also necessary for applications in material synthesis, processing, separations, solar thermal power generation, and energy storage. A round robin was conducted with national laboratory and university participants from twenty-one laboratories in five countries to compare property measurements, to better understand uncertainties, and to identify possible best practices. Two salt mixtures, each from a common batch, were distributed to participants for evaluation: equimolar NaCl-KCl and 45.0LiF-13.7NaF-41.3KF mol % (FLiNaK). Measurements were performed to determine the major constituent composition, oxygen content, density, thermal expansivity, melting point, and thermal conductivity. Error analysis was performed on each measurement for uncertainty quantification for each type of property that was explored. The resulting discussion of the methodologies used in this work is meant to lay the groundwork for the development of standard methods and reference materials for future high-temperature property measurements on halide melts.

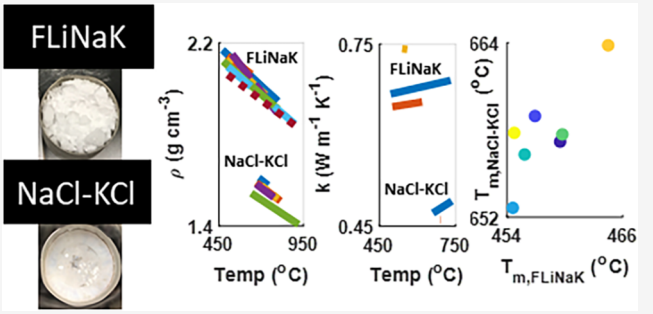

1. INTRODUCTION

Molten salts are cross-cutting technologies for both renewable and nuclear energy technologies, and industries and federal agencies have identified a lack of molten salt chemists and experts in the workforce.[1] These fluids are being developed to serve as coolants and thermal storage media in both concentrated solar power (CSP) and advanced nuclear energy due to favorable characteristics such as high boiling point, low vapor pressure, and high heat capacity.[2] CSP has historically considered alkali nitrate-based salts, whereas nuclear molten salt reactors (MSR) propose halide-based salts (primarily fluorides and chlorides).[3]

Because of their role as heat transfer media, knowledge of the thermochemical and thermophysical properties of molten salts is key to implement them within energy systems. Molten halide salt thermophysical databases, such as Oak Ridge National Laboratory's (ORNL)/University of South Carolina's (USC) Molten Salt Thermal Properties Database – Thermophysical: MSTDB-TP,[4] the University of South Carolina's Molten Salt Thermal Properties Database – Thermochemical: MSTDB-TC,[5] and the European Union's Joint Research Centre Molten Salt Database: JRCMSD,[6] recognize that there are few data on the thermal properties of many molten salts and their mixtures.[7] Additionally, measurements that do exist have been plagued by fundamental

Received: June 23, 2025
Revised: September 30, 2025
Accepted: October 14, 2025

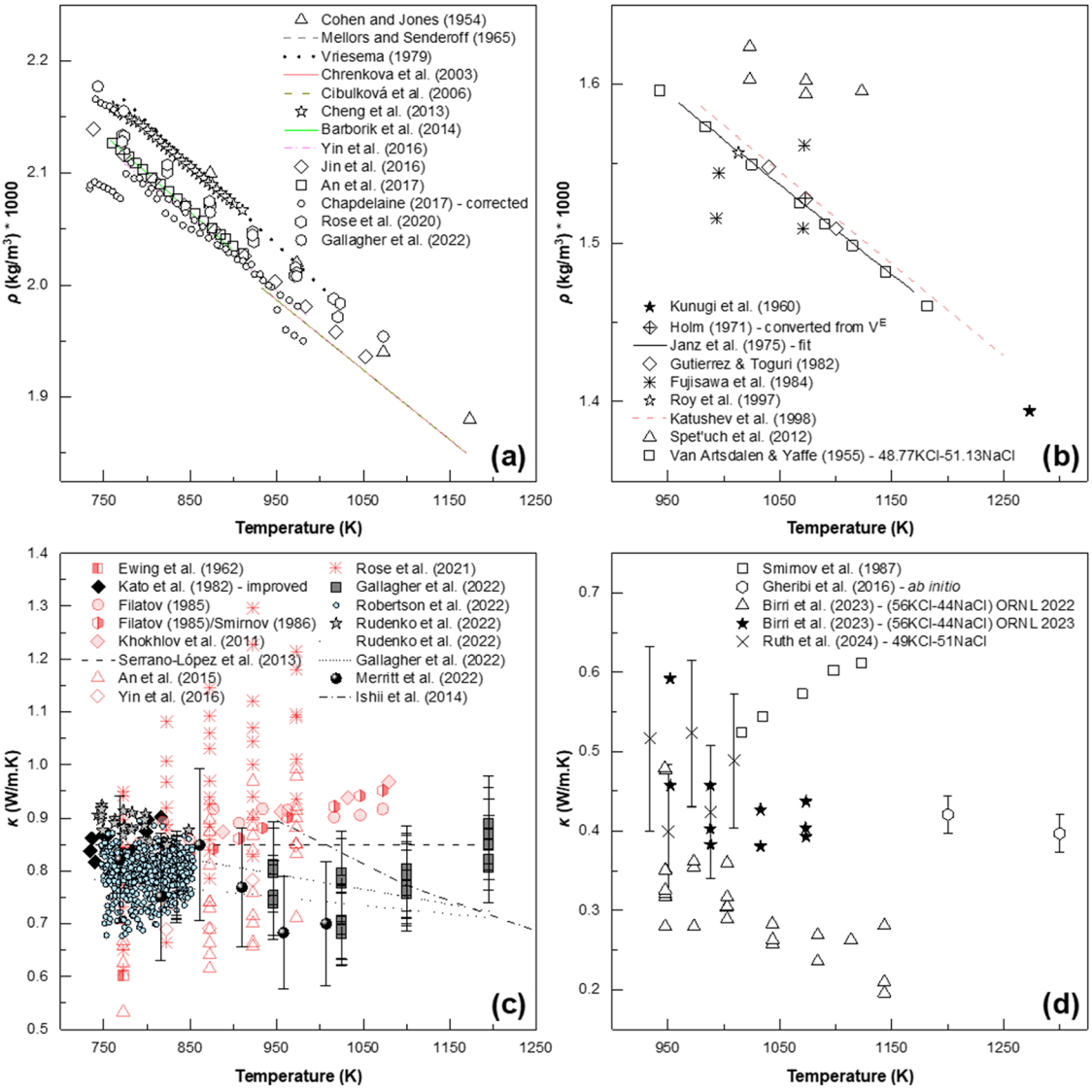

Figure 1. Compiled data for density (a and b) and thermal conductivity (c and d) of the LiF-NaF-KF (FLiNaK) and NaCl-KCl mixtures, respectively. Figures (a, c, and d) are adapted with permission from 11,12. Copyright 2024 Springer Nature and 2024 American Chemical Society, respectively. References for (b) are 13−21.

inconsistency in trends and magnitudes of thermophysical properties (e.g., melting point, density, thermal conductivity, viscosity). This has been further exacerbated by the lack of standard reference materials or measurement standards for high-temperature, electrically conducting fluids, such as molten salt.

Accurate oxygen measurement in molten salts is critical for nuclear applications because even trace oxygen or moisture contamination can severely affect corrosion susceptibility and the salt's redox balance as well as thermophysical properties. Molten salts are used as coolants or fuel media in some reactor designs, and they must be kept highly pure to prevent the corrosion of structural materials. Reliable oxygen analysis helps ensure salt purity, supports corrosion mitigation strategies, and underpins the safe operation of these nuclear systems.

Figure 1 provides a survey of the density and thermal conductivity values for FLiNaK and NaCl-KCl mixtures as illustrative examples, where density measurements are in relatively good agreement compared to thermal conductivity measurements, where even fundamentals such as the temperature dependence (dk/dT) cannot be determined from the data. This discrepancy has been highlighted by multiple sources (Magnusson et al.[8] and Robertson et al.[9]), but the impact of salt composition and impurities compared to experimental methodologies cannot be distinguished because consistent batches of salts have not been available for benchmark testing by multiple laboratories. Even within the same laboratory, Figure 1d shows the impact of experimental design and data analysis on measured data, when comparing ORNL 2022 and ORNL 2023,[10] where the data in 2022 used a variable gap apparatus that lacked heated guards to prevent unwanted radial heat losses, while the 2023 data used a guarded heater. This improvement ensured that the 1D thermal analysis model matched experimental conditions and resulted in data that more accurately match kinetic models. These examples demonstrate the need for a round robin test to help resolve these inconsistencies in salt property measurements and provide general recommendations on the field of thermophysical property measurements of molten salts.

https://doi.org/10.1021/acs.jced.5c00421
J. Chem. Eng. Data XXXX, XXX, XXX−XXX

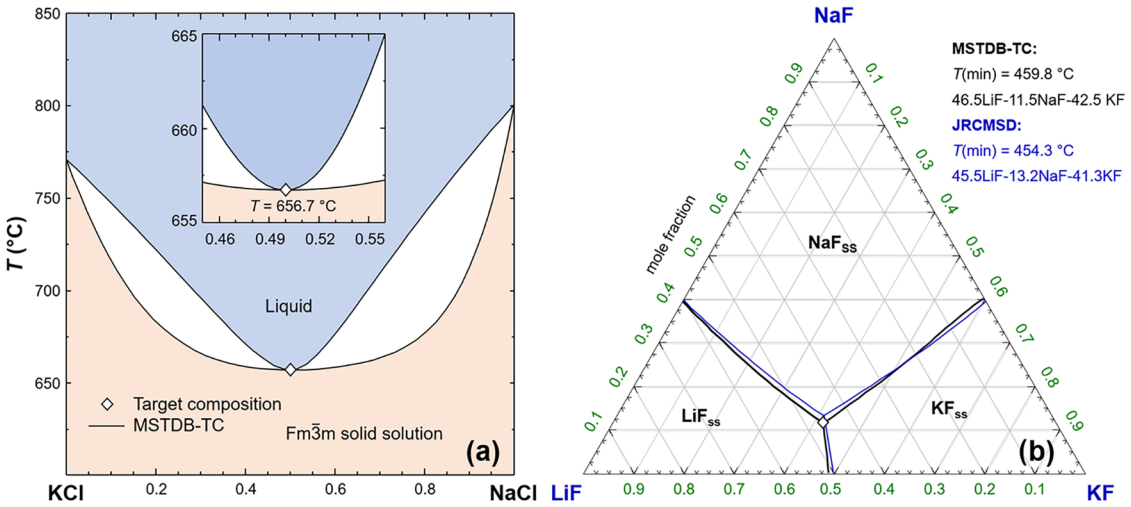

Figure 2. (a) Calculated phase diagram of NaCl-KCl and (b) calculated invariants of LiF-NaF-KF phase diagram with computed eutectic coordinates from MSTDB-TC and JRCMSD databases.

Table 1. Descriptions of the Salt Components: FLiNaK Salt Was the Original Source as an Existing Mixture of LiF, NaF, and KF

chemical name	chemical formula	CAS no.	source	purification method	mass fraction purity
lithium fluoride (in FLiNaK)	LiF	7789-24-4	ECS[a]	likely hydrofluorination	0.109, based on Li ICP-MS
sodium fluoride (in FLiNaK)	NaF	681-49-4	ECS[a]	likely hydrofluorination	0.123, based on Na ICP-MS
potassium fluoride (in FLiNaK)	KF	7789-23-3	ECS[a]	likely hydrofluorination	0.766, based on K ICP-MS
sodium chloride	NaCl	7647-14-5	Fisher Scientific	thermal dehydration	0.995, from the supplier
potassium chloride	KCl	7447-40-7	Sigma-Aldrich	thermal dehydration	0.994, from the supplier

[a]Electrochemical Systems, Inc.

The molten salt round robin study described in this work was created with three main objectives: (1) to quantify uncertainty by identifying common sources of error, demonstrating reproducibility, and identifying limitations of measurement techniques, (2) to share best practices among the experimental groups, and work toward creating a standard methodology, and (3) to establish standard materials through two well-characterized salt lots that can serve as reference material going forward. Although each property required a different measurement approach, this Review aimed to maintain as consistent a style across sections as possible.

The two salts chosen for this experiment were NaCl-KCl (50−50 mol % NaCl-KCl, Figure 2a), and the well-characterized ternary fluoride LiF-NaF-KF (FLiNaK, Figure 2b) with a targeted composition of 46.5−11.5−42 mol % LiF-NaF-KF.

2. EXPERIMENTAL METHODS

2.1. Salt Preparation. Information about the salt components is presented in Table 1. The NaCl-KCl salt mixture (50:50 molar ratio) was prepared at ORNL. A total of 791 g of NaCl (Fisher Scientific, 99.5%) and 1009 g of KCl (Sigma-Aldrich, 99.4%) were mixed as powders and placed in a quartz crucible. The crucible was then loaded into a quartz reactor equipped with a quartz tube under ultra-high purity (UHP) Ar flow. The salt mixture was heated to 850 °C, at which point the quartz tube was immersed in the melt, and UHP Ar was continuously flowed through the salt for 12 h. After this process, the quartz tube was removed, and the salt was cooled to room temperature under UHP Ar. Once cooled, the entire reactor was transferred into an UHP Ar-purged glovebox (O_2 and H_2O < 0.1 ppm), where the salt was ground into small chunks. The processed salt was then packaged in double airtight containers and shipped to collaborators at the University of California, Berkeley, for further distribution. Oxygen analysis was initially attempted at ORNL by the titration method described elsewhere,[22] but the method did not detect any oxygen.

FLiNaK salt, originally sourced from a commercial producer no longer in business (Electrochemical Systems, Inc. (ECS)), was also packaged and shipped to Berkeley. While the exact purification method is unknown due to the supplier company no longer existing, it was likely purified via hydrofluorination, a well-established method in fluoride salt processing.[23,24] This FLiNaK salt was characterized at ORNL using various techniques, including inductively coupled plasma mass spectrometry (ICP-MS), oxygen measurements by inert gas fusion analysis, and corrosion exposure testing.[25,26] This initial ICP-MS analysis was performed prior to distribution of the salt to round robin participants and indicated a composition of 45.0 ± 0.10−13.7 ± 0.05−41.3 ± 0.15 mol % LiF-NaF-KF. The salt was handled inside an UHP Ar-purged glovebox (O_2 and H_2O < 0.1 ppm), crushed into small chunks, and packaged and shipped using the same process as for the NaCl-KCl salt. ICP-MS analysis of the NaCl-KCl salt mixture was not attempted, as batching information was available. Each group measured samples taken directly from the as-received powder that was shipped to each participant.

2.2. Round Robin Methodology. Participants from twenty-one organizations in five countries received salt for measurements, including participants from four DOE laboratories, 14 universities, and three international research

https://doi.org/10.1021/acs.jced.5c00421
J. Chem. Eng. Data XXXX, XXX, XXX−XXX

organizations. Participants were assigned an anonymized participant ID that was used for identifying methods to be applied and for submitting results. The salt properties measured included elemental composition, melting temperature, density, and thermal diffusivity or conductivity.

Information on the measurement methods and conditions used to obtain the properties of salts distributed for the round robin study was collected from each participant using an anonymized form. Several different measurement techniques were employed by different participants for several of the properties, as summarized in Table 2.

Table 2. Techniques Used to Measure Properties of Round Robin Salt Samples

property	test methods
elemental composition	inductively coupled plasma−mass spectroscopy (ICP-MS)
	inductively coupled plasma−optical emission spectroscopy (ICP-OES)
oxygen analysis	inert gas fusion (IGF)
melting point	differential scanning calorimetry (DSC)
density	hydrostatic method
thermal conductivity	laser flash analysis (LFA)
	needle probe
	modulated photothermal radiometry (MPR)

A standard practice for conducting interlaboratory salt studies is available from ASTM (ASTM E691[27]); however, it relies on the participants having used the same test method. Therefore, the statistics recommended for use in the standard practice are not applicable to measurements under this round robin for the measurement of thermal conductivity or diffusivity, where more than one test method was used. Even in cases where participants used the same general method, significant variation in the application of those methods resulted in being unable to use the recommended statistics from ASTM E691.

Analysis of differences in methods used and differences in the application of similar methods can reveal best practices for measuring the properties of molten salts, sources of uncertainty, and causes for differing measured values. It was necessary that information on the methods used by each participant be as complete as possible to facilitate a comparison of measured values and determine causes for differences therein. Organizers of the round robin collected all of the available information from participants on the application of the methods used and presented this in Section 2. Analysis of the effect of differences in the application of methods on measured values can be used as the technical basis for the development of standard test methods for molten salt properties. Participants submitted results in anonymized form using their assigned participant IDs, and those results were collected and are presented in Section 3.

2.2.1. Elemental Analysis. The elemental compositions of the salts were measured by variations of a two-step process: digestion of a sample of salt in acid, followed by ICP-MS or inductively coupled plasma−optical emission spectroscopy (ICP-OES). Of the seven groups reporting elemental composition for FLiNaK, three dissolved the salts with acid in the containers listed in Table 3. In addition to acid digestion, one applied heat by reflux and three used microwave digesters to heat the salt above the standard boiling point of

Table 3. Summary of the Elemental Analysis Parameters; Group 200 Noted That Li Isotopes Were at Their Natural Abundance

group	elem. method	digestion conditions	acids	equipment	standards	salt digested (g)	digest vol. (mL)	# digests	# dilutions	# replicates
124	ICP-OES	microwave in a Teflon vessel	5% v/v of HNO_3	PerkinElmer Avio 200	calibration: Na 1; 2.5; 5 ppm Li & K 1; 2.5; 5; 7.5; 10 ppm	0.01−0.03	8	3	1	2
135	ICP-MS	dissolved in acid in a Teflon beaker	2 mL nitric +1 mL hydrochloric acid	PerkinElmer NexION 2000	performed a blank measurement − did not report standard solutions used	entire sample (0.117−0.174)	50	3	1	3
137	ICP-MS, ICP-OES	dissolved in deionized acidified water	1 mL of concentrated ultrapure HNO_3 +0.2 mL of HCl	PerkinElmer Optima DV 8300;	calibration: 1; 2; 5; 10; 20 ppm for ICP-OES; 1, 5, 10, 50, 100 ppb for ICP-MS	0.120 and 0.104	50	2	2	4
147	ICP-MS	microwave	concentrated nitric and hydrochloric acids, with and without HF	Thermo-Finnigan element 2XR	Li: 4, 20 ppb, 10,000 ppb; Na and K: 80 ppb, 400 ppb, 5000 ppb, 10,000 ppb	0.051− 0.067	50	3	2	3
171	ICP-MS	HNO_3	6 M nitric acid, diluted to 2%	PerkinElmer NexION 1000	calibration standards: Li, Na, K, all at 100, 1000, 10,000 ppb	~0.1	2−5	5	0	3
172	ICP-OES	microwave	6 M nitric acid diluted to 5%	PerkinElmer 5300 DV	inorganic ventures Na, K, Li at 100 ppm	0.136	50	3	3	3
200	ICP-MS	HNO_3, shaken 24 h.	1 M nitric acid	agilent 7800	calibration: Li: 5, 10, 100, 500,1000, 200 ppb, Na: 500, 1000, 2000, 5000, 10,000 ppb, K: 1000, 2000, 5000, 10,000 ppb with check after measurements ensuring <10% deviation through recovery check	0.0071−0.0597	20	6	1	3

https://doi.org/10.1021/acs.jced.5c00421
J. Chem. Eng. Data XXXX, XXX, XXX−XXX

Table 4. Summary of the Density Measurement Parameters, Calibrations, and Environmental Conditions

group	equipment (bob, wire— and crucible materials)	bob mass (g) and wire diameter (mm)	balance calibration& Sensitivity	T calibration& uncertainty	surface tension	bob thermal expansivity (value and citation)	bob volume calibration method, volume value (mL)	thermal equilibration time	heating and cooling	cover gas
122	99.99% Nickel crucible and bob, 26 gauge nickel 200 wire	120.92 g, wire mass 0.46 g and 0.4049 mm	Mettler Toledo MS303TS/00 analytical balance, 0.001 g	type K TC included in setup during measurement- not calibrated	corrected − surface tension coefficients from Janz assumed full wetting (used LiF-KF for FLiNaK)	used temperature-dependent values from Touloukian et al.[32] (accurate to ±3%, per citation)	checked using water displacement, 13.6 mL	~1 h at temperature	random order	Ar, <6.3 ppm of O_2, 0.5 ppm of H_2O (included a daily log)
132	Ni bob, W wire, glassy carbon crucible	9.1803 g and 0.1 mm wire	balance calibrated using NIST weights, 0.001 g	used a K-type TC and a Fluke calibrator, stable to 0.1 °C, accurate to 0.3% T + 1 °C	not accounted for	used temperature-dependent values from specialmetals.com[33]	calibrated in DI water, 1.03 mL	verified constant temperature for >15 min	both	Ar, <10 ppm of O_2, H_2O
135	Ni crucible, bob, and wire	18.6 g and 0.25 mm and 0.5 mm	calibrated using Mettler weights, 0.001 g	pretest calibrated with placeholder salt, to ±2 °C	corrected − used two different-sized bobbers to determine surface tension and temperature dependence	Nickel linear thermal expansion coefficient, 1.3×10^{-5} from Callister[34]	calculated from bob mass and density of nickel, 2.09 mL	>8 h initial melt and >30 min at each temperature	both and random order	in UHP Ar inside a glovebox
169	99.99% Ni bob and wire, alumina crucible	(FLiNaK) 2.0720 g, (NaCl-KCl) 1.7083 g, 0.2 mm wire	calibrated using NIST weights, 0.0001 g	no calibration performed, estimated to be ±20 °C	corrected − determined experimentally using the same wire, different bobs	used slope from the density of nickel by Touloukian et al.[32]	calculated from mass and density	heated at 1 K/min	both	Ar < 2 ppm of O_2 and H_2O
172	Ni 200 Bob, 28 gauge Ni 200 wire	44.41 g[a], 0.32 mm (28 gauge)	phoenix GH-252 analytical balance, 0.00001 g	TC frozen in known salt to measure freezing point offset, ±5 °C	corrected − assumed fully wetting condition	polynomial fit of temperature-dependent nickel thermal expansion coefficient from special metals[33]	used proprietary density calibration fluids, 4.996 ± 0.002 mL	20 min at each temperature	both and random	Ar with <10 ppm of O_2 & <1 ppm of H_2O
179	Pt bob, Mo wire	105.621 g, 0.05 mm	calibrated using weights, 0.001 g	dry block calibrator	corrected	platinum thermal expansion, 9×10^{-6} from Kirby[35]	NIST traceable fluids used to calibrate the bobber volume	1 h between temperature changes. Minimum of 15 min per measurement (4 total at each temp).	both	inert glovebox

[a]Calculated from given volume at 25 °C and published density for Ni200 (8.89 g/mL).

https://doi.org/10.1021/acs.jced.5c00421
J. Chem. Eng. Data XXXX, XXX, XXX−XXX

the acids at ambient pressure (for example, up to 190 °C for group 147). Of the four groups that reported elemental composition for the NaCl-KCl mixture, one dissolved the salt for 24 h, one applied heat by reflux, one performed an oven digestion, and one performed a microwave digestion above the boiling temperature of the acids at ambient pressure (similar to the measurement of FLiNaK). Elemental analysis details are presented in Table 3.

2.2.2. Oxygen Analysis. Inert gas fusion (IGF) is a high-temperature combustion method used to determine the oxygen content in salt samples. The sample is heated to extremely high temperatures (up to 3000 °C) in a graphite crucible under an inert carrier gas that also can contain a flux material, such as short, nibbled nickel, for better conductivity. At these temperatures, oxygen in the salt reacts with carbon from the crucible or additionally added graphite powder, forming carbon monoxide (CO) and carbon dioxide (CO_2). The evolved gases are then carried by the inert gas stream into a detection system, typically infrared (IR) sensors. This fundamental mechanism is consistent across different commercial oxygen analyzers by various analyzer brands such as LECO,[25,28] Bruker,[29] or Eltra.[30]

Calibration curves are developed using standard materials such as titanium pins with known oxygen content, with results typically reported in parts per million (ppm) by weight (i.e., μg/g). IGF analysis is rapid, with some level of sample preparation, such as encapsulating the salt in capsules in an inert atmosphere glovebox and grinding the salt into powder with a mortar and pestle. IGF analyzers can detect oxygen at low levels (<1 ppm), making it a reliable method for determining oxygen in salts used in nuclear applications.

2.2.3. Density. Although the method was not prescribed, all six groups that performed density measurements used a hydrostatic method based on the Archimedean principle, which states that the buoyant force of an object submerged in a fluid is equal to the weight (and by extension, the mass) of the displaced fluid.[31] By monitoring the apparent mass of a bob of known volume and expansivity suspended in a molten salt, the density of the molten salt can be calculated using the following relation:

$$\rho = \frac{m - m'}{V} \tag{1}$$

In eq 1, ρ is the density of the molten salt, m is the true mass of the bob, m' is the apparent mass of the bob submerged in the salt, and V is the volume of the bob. The volume expansion of the bob is typically accounted for by a linear approximation:

$$V(T) = V_0(1 + 3\alpha(T))T \tag{2}$$

where V_0 is the volume at a reference temperature, α is the linear expansion coefficient, and T is the temperature. Surface tension exerts a force on the suspension wire during measurement, as well. A surface tension correction can be added to the numerator of eq 1, as in eq 3, where D is the diameter of the wire, g is the acceleration due to gravity, θ is the contact angle of the salt at the wire, and σ is the surface tension coefficient. It is generally assumed that salts wet the nickel wires used, and therefore $\cos(\theta) = 1$. Table 4 presents a summary of reported experimental method details, instruments used, and density measurement conditions for each participant.

$$\rho(T) = \frac{\Delta m + \left(\frac{\pi D\sigma \cos(\theta)}{g}\right)}{V_0[1 + \alpha T]^3} \tag{3}$$

All participants performed measurements under an inert atmosphere and at both ascending and descending temperatures or in a random temperature order to prevent hysteresis effects.

Differences in the application of the Archimedean method can result in differing measured values. Differences in application among the participants include the relative size of the bobber and wire, whether surface tension corrections were applied, the linear thermal expansion coefficient value selected for the nickel bob, and the equilibration time.

A consistent set of surface tension values for FLiNaK salt are not available, which caused one participant to substitute the surface tension value of a similar salt, LiF-KF,[36] to account for the effect of surface tension in their measurements. Other participants made measurements with different bob and wire sizes to self-determine the surface tension contribution, as shown in eq 4. While surface tension can be corrected for if the coefficient is known, it is best to minimize its effect and therefore any contribution to uncertainty due to uncertainty in the surface tension coefficient value. The use of a thin wire and a bob of large mass minimizes the effect of surface tension force on m'.

$$\rho = \frac{\Delta m_1 + \frac{\pi D_1\sigma}{g}}{V_0[1 + \alpha T]^3} = \frac{\Delta m_2 + \frac{\pi D_2\sigma}{g}}{V_0[1 + \alpha T]^3} \tag{4}$$

Minimizing the relative effect of the surface tension by using a thin wire will prevent the need to determine the surface tension effect and correct for it. Materials with low thermal expansivity should be used to minimize the change in the bob and wire volume with temperature. All participants used nickel bobs and wires, with the exception of participant 132, who used a tungsten wire, and participant 179, who used a platinum bob and molybdenum wire. Different values for the thermal expansion coefficient of nickel were used by the participants, using nickel bobs, with some using temperature-dependent correlations from literature and others using constant values. These values and correlations are shown in Figure 3, where lines represent correlations or constant values obtained from the literature, and points represent discrete values at selected temperatures obtained from the literature. At 900 °C, participant 122 used a thermal expansion coefficient value of

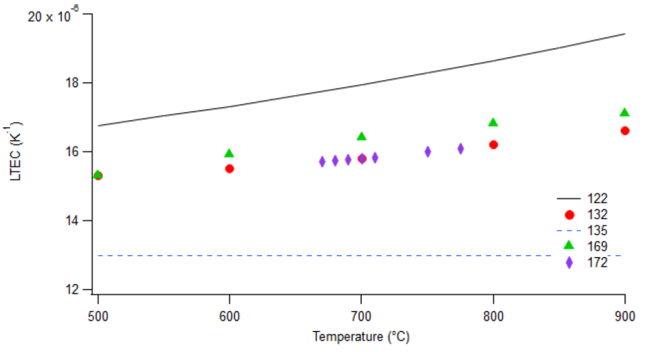

Figure 3. Linear thermal expansion coefficients for nickel used by participants in determining density values from measured masses, as cited in Table 4.

https://doi.org/10.1021/acs.jced.5c00421
J. Chem. Eng. Data XXXX, XXX, XXX−XXX

Table 5. Summary of the DSC Parameters

group	equipment	crucible	sample size (mg)	ground?	% weight change	interpretation method	calibration standards	selected rate for the heating program (°C/min)	DSC cover gas	*N* samples	*N* ramp
124	Netzsch 404 F3 Pegasus	SS, Ni liner	20−40	yes	0	extrapolated onset	In, Sn, Bi, Zn, NaCl-KCl, KF, Ag, and Au	1, 3, 5, 10	99.999% Ar	1	1 for each heating rate
125	Netzsch STA F449 F1 Jupiter	Netzsch SS316 L crucible, Ni-201 liner/lid	40−50	yes	sealed; no change	interpolation of onset	In, Sn, CsCl, K_2SO_4, $BaCO_3$, Ag, and Pb	5	99.99% Ar, Oxygen trap system (OTS)	1	3
128	Netzsch STA 449 F3 Jupiter	glassy carbon	20−50	no		onset interpolation, Netzsch software	Bi, Sn, Zn, Al, Ag, and Au	5, 10, 15, 20	Ar	1	4, one per scan rate
135	Netzsch STA 449C	hermetically sealed Au	∼25	yes	sealed cells − no change	onset interpolation	Calibrated with Ag, Au, Sn, Zn, and Al, $T \pm 2$ °C	5	Ar	3	2 each
137	Netzsch DSC 404	Netzsch SS316 L crucible, Ni-liner, and lid	∼20	yes	sealed cells − no change	onset interpolation	In, Sn, Bi, Pb, CsCl, Al	5	Ar	6 (FLiNaK) 2 (NaCl-KCl)	4
169	Setaram MDHTC96	SS, Ni liner	∼50		sealed cells − no change	onset interpolation	In, Sn, Pb, Zn, Al, Ag, Au	2, 10, 10	Ar	1	3 each
171	Mettler Toledo model 822e	aluminum, pierced lid	4−7.9	yes	0	onset; STARe v9.00 software	In, Zn	5, 10, 15	Ar	8	2−4
180	Setaram 96 line multi HTC	SS crucible, Ni liner, closed	∼60	yes	sealed cell − no change	onset interpolation	In, Sn, Pb, Al, Ag, Au	2, 4, 6, 8, 10, 12	Ar	1	4
193	Netzsch DSC 404F1 Pegasus	SS crucibles, Ni lid	20−25	yes	sealed cells − no change	onset interpolation	In, Pb, CsCl, Ag, and BaCo	5	Ar	1	4

https://doi.org/10.1021/acs.jced.5c00421
J. Chem. Eng. Data XXXX, XXX, XXX−XXX

1.94×10^{-5} K^{-1}, while participant 135 used a value of 1.3×10^{-5} K^{-1} at the same temperature for the same material. The use of different thermal expansion coefficients contributes to the differences in measured values.

Participants must determine the bob volume at room temperature to calculate the density of salts from the measured bob masses at other temperatures. Two participants measured the bob volume in water, two participants calculated the volume from measured mass and published nickel density values, and two participants used proprietary or NIST fluids to determine the volume of the bob. Each method of determining bob volume will have different sources of uncertainty, contributing to differences in measured values.

Sufficient equilibration time should be allowed so that measurements at a single temperature made in ascending and descending temperature order or in random temperature order are consistent. Replicate measurements in ascending and descending temperature order were made by all of the participants, and some made measurements in random temperature order.

Maintaining the salt composition throughout the measurement is necessary to compare the measured values. Corrosion-resistant crucible, bob, and wire materials were selected by all participants, and all salt handling and measurements were conducted in low-oxygen and moisture-free environments.

Aspects of the measurement that contribute to measurement uncertainty include uncertainty in the salt composition, temperature, and mass of the bobs. Additional sources of uncertainty include uncertainty in the coefficients used to calculate the density, including the thermal expansion coefficient and surface tension coefficient. The measured salt composition was initially identical for all groups, as all salt aliquots originated from a single batch, but variations in salt handling may have altered the salt composition. All participants reported their salt handling inside inert atmosphere gloveboxes, but to varying levels of the oxygen and moisture content. All participants used corrosion-resistant materials, and because of this, the composition of salts used in this study is likely to have remained unchanged.

Participants reported different means of measuring temperature, including participants 135 and 172 using a pretest determination, correlating furnace setting with in-crucible temperature, and participants 122, 132, 169, and 179 using a thermocouple during measurements. Using a thermocouple during measurements provides a real-time measurement of the salt temperature, but it can become a heat sink, creating temperature gradients in the salt.[37] A comparison of these two methods to determine the best practice will be useful.

2.2.4. Melting Point. Although the method was not prescribed, all groups performed melting point measurements by DSC. Principally, DSC is loaded with two crucibles of the same type, one with a sample to be measured and one empty reference crucible. In some cases, the reference crucible may also contain a reference material with a transition temperature that will not overlap with that of the sample. Such a configuration allows for the determination of transition enthalpies of unknown materials. DSC instruments can operate in one of two modes: heat-flux mode, in which the voltage difference between the thermocouples (around or below the sample and reference crucibles in 3D and 2D heat-flux measurements, respectively) is measured to describe the apparent heat flow of the sample, or power compensation mode, in which each crucible is heated independently and the power difference needed to hold the crucibles at equal temperatures is measured to describe the apparent enthalpy change. The mode of operation is instrument-specific and is not often noted in methodologies. In either case, heat supplied to the sample is graphed against time or temperature, and the occurrence of a peak indicates a transition within the sample.

A solidus is determined from an interpolated onset of the endothermic peak upon heating; conversely, the liquidus is determined upon heating from the last heat flow peak resembling a shoulder by either taking the peak maximum or the offset of this shoulder. The liquidus could also be determined on cooling from the onset of the freezing event. However, it is important to note that halide salts exhibit significant supercooling behavior. As a result, DSC measurements taken during cooling programs may significantly underestimate the transition temperatures.

Reference materials with well-characterized (congruent) melting points and of high purity are used as calibrants (e.g., In, Sn, Pb, Al, Ag, Au), whereby the temperature difference between the measured and true melting points (taken as the onset of the interpolated heat flow peak) is determined as an instrumental offset. The measurement of several standards, spanning a wide temperature range, produces a calibration curve that describes "true transition temperatures" after correction for instrumental and measurement conditions effects. This temperature offset is unique for each instrument, depending on the geometry and on the heating rate applied.

While each group has its own method to prepare material samples, some generic procedures are described here. Sample preparation typically takes place within an inert atmosphere glovebox. Salts are typically dehydrated to remove any residual impurities (in the current case, potentially absorbed moisture), which may be done through a simple heating process at elevated temperatures (typically around 300−400 °C). A target sample mass is placed into a crucible, which can be challenging, given the small masses involved. Some groups used an encapsulated crucible for DSC measurements for the purposes of preventing sample contamination with air during the measurement and to prevent sample vaporization at high temperature, which can lead to composition change due to incongruent vaporization and subsequently to prevent damage to sensitive detectors. For the former reason, the encapsulation process is performed within the glovebox prior to crucible removal from the antechamber if removal is necessary. A common challenge is that there are no commercially available crucibles compatible with salts that can withstand temperatures above 700 °C, which is why some groups used a custom design with a nickel liner (or other chemically compatible sleeve such as graphite or oxygen-free BN) and stainless steel base to ensure hermetic tightness at elevated temperatures.[38,39] A summary of DSC experimental parameters appears in Table 5, which indicates the group number, vendor, and model of instrument, crucible design, sample size, preparation method, interpretation method, calibrants, heating rate during measurements, number of samples, and number of heating cycles.

2.2.5. Thermal Conductivity. Four participants measured the thermal conductivity and/or thermal diffusivity of the distributed salts. Two used a laser flash method, one used a periodic laser heating method, and one used a needle probe method. The details of the methods used by participants are provided in Table 6, including information on environmental controls, calibrations, and any corrections applied. The dissimilar methods used will prevent a robust discussion of

https://doi.org/10.1021/acs.jced.5c00421
J. Chem. Eng. Data XXXX, XXX, XXX−XXX

Table 6. Summary of Thermal Conductivity Experimental Parameters; (Weight Loss Was Not Measured)

group	method	temp. calibration and range	sample mass (g)	container material	corrections	standards and applicable temp. range	cover gas
135	laser flash at the bottom of the sample, temperature recorded at the top – measured diffusivity, used measured density and heat capacity to calculate thermal conductivity	determined accuracy using the melting point of reference salt, ± 5 °C	1–2, measured three samples with 3 shots each	graphite	thickness of the sample. the thermal model includes radiative heat transport.	molybdenum reference metal sample provided by the manufacturer, between RT and 1000 °C	flowing UHP Ar, cells prepared in glovebox under UHPO Ar with <10 ppm of O_2, <1 ppm of H_2O,
137	laser flash method[40]	determined using the Fe standard and provided by the manufacturer	0.15–0.2	graphite	the thermal model includes conductive, radiative heat transport, finite pulse width, and heat losses	poco graphite standard provided by the manufacturer, and thermal conductivity of KNO_3 compared to the reference correlation[41]	Ar, O_2 $<10^{-9}$ ppm encapsulated salt prepared in inert glovebox with O_2 < 3 ppm, H_2O < 10 ppm
166	periodic laser heating, density, and heat capacity from literature	IR calibration against Lumasense technologies IGA 320/23- LO pyrometer	0.2	inconel 625 with Pt coating, Pyromark 2500 coating	radiation heat loss from the surface, natural convection limited due to modulated heating and low Nusselt number	paraffin wax (100 °C), sulfur (250 °C), KNO_3 compared to reference correlation[42]	Ar
187	needle probe sensor	thermocouple calibrated against a PT100 platinum resistor placed next to the needle probe within the furnace	3	Ni-200	the thermal model includes radiation heat transfer through salt, convection limited by a narrow annulus	thermal conductivity of water, $NaNO_3$, KNO_3 (up to 400 °C) compared to reference correlations[41,43−45]	Ar, O_2 < 3 ppm

best practices for any one method and prevent the use of ASTM E691 for analysis of the results.

The laser flash analysis (LFA) technique was first developed in the 1960s to measure the thermal diffusivity of solid materials.[46] Applying the technique to fluids requires encapsulating the sample between two parallel surfaces, often within a crucible, impinging a laser-induced heat pulse on one surface,[47] and measuring the temperature response on the opposite surface as a function of time. This is commonly accomplished by recording the relative increase in the intensity of the emitted infrared light as the surface temperature increases. The effective thermal diffusivity of all three layers is determined from the resulting thermogram, and the thermal diffusivity of the fluid sample then needs to be isolated from the contributions of the crucible. Using materials with a much higher thermal conductivity can reduce the impact of the crucible material on the measurements. The thermal conductivity (k) of the fluid is then determined indirectly using specific heat (c_p) and density (ρ) and the relationship $\alpha = k/\rho c_p$, or it is estimated by matching simulated and experimental thermograms. The thermogram simulations were produced using finite element analysis (FEA) to predict conductive and radiative heat transport, and heat loss accounting for the geometry of a 3-layered system. For molten salts, LFA crucibles are designed to minimize radial heat flow between the top, bottom, and sides portions to ensure that heat is primarily transferred through the salt instead of the more conductive crucible. Convective heat transfer from the fluid is minimized by the crucible design.[48,49] The thickness of the salt in the crucible can be determined by micrometer and confirmed by X-ray computed tomography to ensure the salt and crucible represented a 3-layered system for laser flash analysis.

Thermal conductivity measurements by periodic laser heating rely on measuring the impact the modulation frequency of the laser has on the resulting temperature variations within the substrate that the fluid is in contact with at the same frequency.[50] This approach measures the thermal effusivity ($e = \sqrt{\rho c_p k}$) using modulated photothermal radiometry (MPR).[51] The k of the molten salt is then determined by $k = \frac{e^2}{\rho c_p}$. The ρc_p values are extracted from the literature, as in the laser flash technique, where conductivity is obtained from measured diffusivity. The amplitude and decay of these thermal waves (temperature variations) are fit to a thermal model to determine the thermal effusivity of the fluid. Laser intensity can be modulated in a continuous sine wave[42] or by pulsing the laser,[52] and the thermal response of the substrate is detected by modulations in the emitted infrared light from the front surface. The heat is applied to the top of a three-layer structure: Pyromark coating: thin Inconel 625 sheet − molten salt layers. The Inconel sheet is 100 μm thick, and its side in contact with the molten salt is coated with a thin (∼200 nm) layer of Pt to avoid corrosion. The surface temperature oscillation of the sample is monitored by a pyrometer. A pair of parabolic mirrors focused the infrared signal from the samples to the detector. The thermal response signal received by the HgCdTe (MCT) detector is then collected by a lock-in amplifier, while the signal from the function generator serves as the reference signal. At the low-frequency limit, the surface temperature oscillation θ_s shows a linear relation with $\omega^{-1/2}$, where $\omega = 2\pi f$. The slope of θ_s versus $\omega^{-1/2}$ is proportional to the inverse of the thermal effusivity of molten salt e_f, i.e., $\frac{1}{e_f}$. By

https://doi.org/10.1021/acs.jced.5c00421
J. Chem. Eng. Data XXXX, XXX, XXX−XXX

Table 7. Elemental Composition: Major Cations in FLiNaK[a]

grp	digestion method	analysis method	n		Li/LiF	Na/NaF	K/KF	total major constituents
124	microwave digestion	ICP-OES	3	wppm	77,800 (1600)	63,400 (6000)	3,99,300 (10,500)	5,40,500 (10,500)
				wt %	29.1 (3)	11.6 (6)	59.3 (1.1)	98 (2)
				mol %	**46.4 (4)**	**11.4 (6)**	**42.2 (8)**	*100*
				the residual standard deviation of the N runs was multiplied by the corresponding student coverage factor to estimate the errors				
135	dissolved and refluxed in HNO_3 and HCl	ICP-OES (majors)	3	wppm	80,000 (1800)	63,900 (1300)	3,81,000 (11,000)	5,25,000 (12,000)
				wt %	29.9 (7)	11.7 (2)	56.7 (1.7)	98 (2)
				mol %	**47.9 (1.3)**	**11.5 (3)**	**40.6 (1.4)**	*100*
137	dissolved	ICP-OES (majors)	2	wppm	77,000 (6000)	65,000 (4000)	4,00,000 (30,000)	5,40,000 (30,000)
				wt %	29 (2)	11.8 (8)	59 (4)	99 (5)
				mol %	**46 (4)**	**11.6 (1.0)**	**42 (4)**	*100*
				errors are propagated from self-reported error estimates				
147	microwave digestion	ICP-MS	3	wppm	71,300 (1300)	69,000 (2000)	3,90,000 (19,000)	5,31,000 (19,000)
				wt %	26.6 (5)	12.6 (4)	58 (3)	97 (3)
				mol ratio	**44.1 (1.3)**	**12.9 (5)**	**43 (2)**	*100*
171	dissolved	ICP-MS	1	wppm	67,000 (9000)	60,000 (8000)	3,70,000 (70,000)	5,00,000 (70,000)
				wt %	25 (3)	10.9 (1.4)	56 (11)	92 (11)
				mol %	**44.3 (6)**	**11.9 (6)**	**43.8 (1.1)**	*100*
172	microwave digestion	ICP-OES	1	wppm	67,000 (2000)	57,000 (2000)	3,37,000 (13,000)	4,60,000(13,000)
				wt %	25.1 (8)	10.3 (4)	50.1 (1.9)	85 (2)
				mol %	**46.6 (1.8)**	**11.8 (5)**	**41.6 (1.8)**	*100*
				errors are propagated from the calibration fit parameter and dilution errors				
200	dissolved, shaken for 24 h in HNO_3	ICP-MS	6	wppm	76,100 (1100)	63,100 (800)	4,06,000 (3000)	5,45,000 (3000)
				wt %	28.4 (4)	11.52 (0.15)	60.4 (4)	100.4 (6)
				mol %	**45.2 (0.4)**	**11.4 (0.1)**	**43.3 (0.4)**	*100*

[a]Except where otherwise noted, errors given in () represent margins of error at 95% confidence. Italicized values indicate that 100% is arrived at by default, due to the choice of denominator.

Table 8. Elemental Composition Results: Major Cations in NaCl-KCl-Eutectic[a]

grp	digestion method	analysis method	n		Na/NaCl	K/KCl	total major constituents
nominal NaCl-KCl[58]		**wppm (g cation/g sample)**			**1,73,000**	**2,94,000**	**4,67,000**
		wt % (g Cl salt/g sample)			**43.9**	**56.1**	*100*
		mol ratio (per (Na+K))			**50**	**50**	*100*
135	dissolved and refluxed in HNO_3 and HCl	ICP-OES (majors)	3	wppm	1,69,000 (5000)	2,84,900 (1500)	4,54,000 (5000)
				wt %	42.9 (1.2)	54.4 (3)	97.3 (1.2)
				mol %	50.1 (1.5)	49.9 (7)	*100*
147	oven digestion	ICP-MS	3	wppm	1,76,000 (8000)	3,20,000 (40,000)	5,00,000 (40,000)
				wt %	44.8 (1.9)	62 (7)	107 (8)
				mol %	50 (4)	50 (7)	*100*
172	microwave digestion	ICP-OES	3	wppm	1,67,000 (2000)	2,76,000 (4000)	4,43,000 (5000)
				wt %	42.3 (6)	52.8 (9)	95.1 (1.1)
				mol %	50.5 (9)	49.5 (1.0)	*100*
200	dissolved, shaken for 24 h in HNO_3	ICP-MS	6	wppm	1,69,000 (2000)	3,00,000 (3000)	4,68,000 (3000)
				wt %	42.8 (5)	57.2 (5)	100.1 (7)
				mol %	48.8 (0.5)	51.2 (0.5)	*100*

[a]Except where otherwise noted, errors given in () represent margins of error at 95% confidence. Italicized values indicate that 100% is arrived at by default, due to the choice of denominator.

using a differential method, e_f can be obtained by comparing the measured layer with a known reference sample. In this work, borosilicate glass is chosen as the reference.

The needle probe technique for measuring the thermal conductivity of molten salts is based on measuring the transient temperature rise at the center of the needle when a wire within the needle is heated at a constant voltage.[53] This centerline temperature is measured by a Type K thermocouple placed between the heating wires within the needle. The heating wire wraps around the length of the sensing region of the probe, and the thermocouple and heating wire are electrically insulated by a ceramic material, often alumina.[54] The probe is then sheathed in a corrosion-resistant metal for protection. The temperature of the thermocouple is impacted by the thermal conductivities of the surrounding materials, where less conductive materials result in higher thermocouple temperatures. Needle probes have successfully been used to measure the thermal conductivity of solid materials,[55,56] but implementing the technique for molten salt measurements requires additional considerations. The most important

https://doi.org/10.1021/acs.jced.5c00421
J. Chem. Eng. Data XXXX, XXX, XXX−XXX

Table 9. Oxygen Content of FLiNaK and NaCl-KCl Eutectic[a]

group	analysis year	analyzer model	encapsulation of samples done in a glovebox?	samples ground into powder?	sample mass (mg)	analysis temperature (°C)	LOD (ppm)	FLiNaK		NaCl-KCl	
								n	O wppm	*n*	O wppm
135	2021	LECO 836	yes	as-received salts in powder form	100 ± 1	N/A	±40% for NaCl-KCl ± 25% for FLiNaK	5	1865 (439)	4	450 (171)
137	2024	LECO O836	yes	yes, with an agate mortar and pestle	100 ± 1	N/A[b]	0.3	4	489 (16)	3	208 (47)
200	2024	Bruker G6 Leonardo	yes	yes, with an agate mortar and pestle	100 ± 1	2800	0.3	3	466 (54)	3	339 (45)

[a]Note: Values in () represent the standard deviation across different samples of that group. [b]Furnace Power: 4800 W.

modifications include limiting convective currents in the salt by limiting the thickness of the salt to an annulus of hundreds of μm thick around the probe.[11] The small gap ensures that viscous forces dominate buoyant forces, which allows convective heat losses to be ignored. Finally, the thermal model used in the needle probe technique needs to include radiative transport through the molten salt at high temperatures to ensure that the measured thermal conductivity is only impacted by conductive heat transport.[57] If these conditions are not met, the measured thermal conductivity will be biased high due to convective and radiative heat transport, which increase the rate of heat transfer and are not accounted for by the thermal models, which assume that all heat transfer is through conduction.

Because there is no high temperature standard reference fluid, participants compared thermal conductivity measurements to solid materials (molybdenum for 135 and poco graphite for 137) and fluids (water for 187, paraffin wax and sulfur for 166, and $NaNO_3$ and/or KNO_3 for 137, 166, and 187) to act as a consistent material for comparison (see Table 6). Participants also needed to account for nonconductive heat transfer modes, such as radiation and convection. All groups include radiative heat transport in the thermal analysis model either analytically or numerically. Convective heat transport is included in the thermal model of 137, while 166 and 187 minimize convection through experimental design meant to limit Rayleigh and Nusselt numbers.

Temperature calibrations were determined against standard material melting points (salt for 135 and iron for 137), blackbody radiation via pyrometer (166), and platinum resistor (187). All salts were tested under argon atmospheres in graphite (135, 137), platinum-coated Inconel 625 (166), or Ni-200 (187) containers to limit salt corrosion.

3. RESULTS AND DISCUSSION

3.1. Results. *3.1.1. Bulk Composition.* Elemental analysis results for major cations are listed in Table 7 for FLiNaK and in Table 8 for NaCl-KCl eutectic, respectively. In both tables, weight parts per million (wppm) refers to the mass of each cationic element detected by ICP analysis per mass of the sample. Weight percent (wt %) refers to the estimated mass of the corresponding fluoride salt (e.g., Li as LiF), assuming the most likely oxidation state and compound form for the cation, relative to the total sample mass. Anions are not measured by ICP spectroscopy and are inferred based on the expected chemical composition of the salt. The mole ratio is calculated out of the major constituents only: LiF, NaF, and KF for FLiNaK; and NaCl and KCl for the chloride salt eutectic. Self-reported errors in the measurements are reported in the parentheses next to the measured values for each participant. The number of replicates (n) refers to the number of digests performed on each salt. Tables S-1 and S-2 in the Supporting Information report the density and melting point of several LiF-NaF-KF compositions as a reference, while Section 1 discusses the target composition of FLiNaK in this study.

The sum of the wt % of each constituent is equivalent to the percent recovery. For FLiNaK, percent recovery is statistically compatible at 95% confidence with complete recovery for five out of six groups. For the NaCl-KCl mixture, percent recovery is statistically compatible at 95% confidence to complete recovery for two out of four groups. For both salts, microwave digestion does not result in a higher digestion efficiency. Group 172 reports lower recovery for both salts despite use of a microwave digester. In cases in which the digestion efficiency is less than 100%, concentrations of trace constituents are near or below detection limits and are insufficient to explain the missing mass. The reported minor constituents are inconsistent across groups. For example, Group 135 reports 200 wppm of Ca and Group 147 reports 60 ppm of Ca; Group 135 reports 10 wppm of Be and Group 147 reports 10 wppb Be. A complete list of minor constituents present in the salt for each group is provided in the Supporting Information.

It should be noted that measurements by ICP-MS and ICP-OES do not show differences when analyzing major constituents like Na, K, and/or Li. Additionally, groups that used a mixture of nitric acid and hydrochloric acid obtained results similar to those groups that used only nitric acid, which seems to indicate that the choice of acid did not have a large impact on the results.

3.1.2. Oxygen Analysis. Results of the oxygen content measurements are presented in Table 9. The number of replicates (n) refers to the number of samples measured from each salt. For FLiNaK, which had three participants, the oxygen concentrations were comparable for groups 137 and 200; however, there was a large deviation in comparison to group 135, which also reported a much higher limit of detection (LOD). One major difference between the salt received by group 135 was that the as-received salts were already in powder form, while group 200 received salts from group 137, where both salts were in solid chunks and further ground down into powder in gloveboxes and then encapsulated in tin capsules. A notable difference found in NaCl-KCl salt was that all groups were comparable, taking into consideration the standard deviation across different samples from a single group (in parentheses in Table 8). The concentration of oxygen is reported in weight ppm (wppm),

https://doi.org/10.1021/acs.jced.5c00421
J. Chem. Eng. Data XXXX, XXX, XXX−XXX

defined as the amount of oxygen in micrograms (μg) per gram (g) of salt.

3.1.3. Density. The measured densities of the distributed compositions of FLiNaK and NaCl-KCl salts from all participants appear in Figures 4 and 5 (respectively) as points.

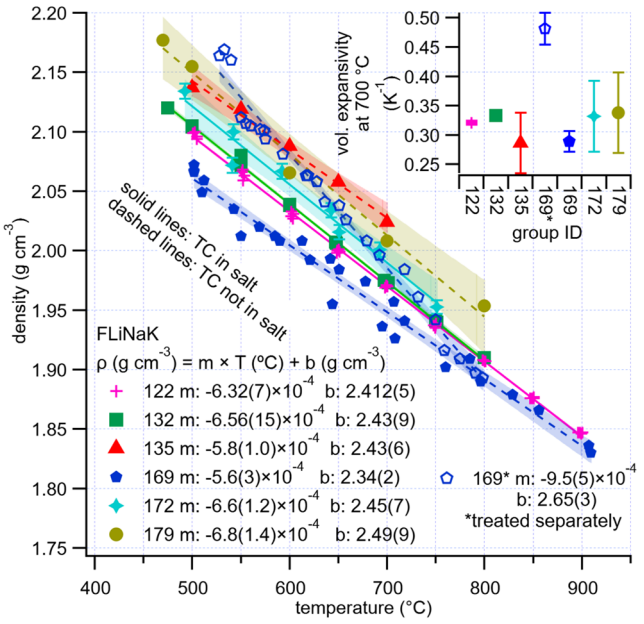

Figure 4. Temperature-dependent densities of FLiNaK. Linear fit parameters are shown in the legends, with the error in the final digit in parentheses. Error bands are 95% confidence bands of linear fits. Solid lines indicate measurements with thermocouples in direct physical contact with the salts. The thermal expansivity of FLiNaK is shown in the upper right inset. 169* was treated separately due to large slopes. Tabulated values of density measurements are reported in Table S-3 in the Supporting Information.

Linear regression was performed on all data sets and appeared as lines in the same color as the measured value points, with fitting values provided within the figures and in Table 10. These linear regressions were used to determine the thermal expansivity, shown in the insets of Figures 4 and 5, as a ratio of the slope of the regression line to the computed density at the specified temperature. The shaded regions associated with each data set represent 95% confidence bands for the linear fit to the data. Self-reported uncertainty, if available, can be found in the Supporting Information. Due to the inconsistency in reporting of uncertainty, these values are not directly compared here.

Participants 122 and 169 reported multiple sets of measurements. All data from participant 122 showed similar trends and, therefore, were pooled before linear regression. For participant 169's measurements of FLiNaK, two sets of measurements were performed, and each measured density on both the heating and cooling ramps. Whereas the data on the first cooling ramp were consistent with the second heating and cooling ramps, the data from the first heating ramp exhibited different slopes and intercepts. Therefore, the FLiNaK data from participant 169's first heating ramp are plotted and regressed separately.

Random sources of uncertainty for density measurements include the sensitivity of the measurement devices, including the balance, thermocouple, and, if dimensions are used to estimate volume, any dimension measuring devices. These sources of error are tabulated if available in Table 3 (see

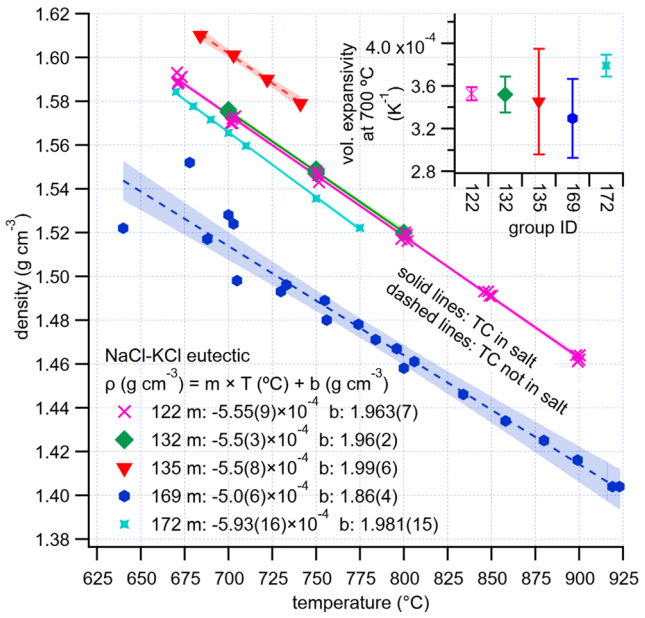

Figure 5. Temperature-dependent densities of the NaCl-KCl mixture. Linear fit parameters are shown in the legends, with error in the final digit in parentheses. Error bands are 95% confidence bands of linear fits. Solid lines indicate measurements with thermocouples in direct physical contact with the salts. The thermal expansivity of NaCl-KCl is shown in the upper right inset. Tabulated values of density measurements are reported in Table S-3 in the Supporting Information.

Section 2.2.3). For density, the total uncertainty is dominated by systematic errors in temperature, linear thermal expansion of the bob, and surface tension effects on the wire, all of which drive density to lower values. For both salts, the lowest densities are measured by participant 169. However, all participant data, except the anomalous second set of measurements from participant 169, show similar trends with temperature having regression line slopes of between 5.6 × 10^{-4} and 6.8 × 10^{-4} g cm^{-3} °C^{-1}. This indicates contributions to the systematic errors from surface tension and volume expansion of bobbers are likely negligible despite differences in approach, as these factors would change the temperature dependence of the measured density, as they are themselves temperature-dependent. The variation in the linear thermal expansion coefficient between its maximum and minimum ranges, as seen in Figure 3 (see Section 2.2.3), changes the thermal expansivity by 2 × 10^{-5} g cm^{-3} °C^{-1} and the volume of the bob by 3.15% and therefore the density by at most 1.3%.

Participants provided values for wire diameter and bob mass from column 3 in Table 4 (see Section 2.2.3) and surface tension correlations for NaCl-KCl from Janz, and a 50/50 LiF-KF correlation from Janz can be used to estimate the relative contribution of surface tension to the measurement. The force contributed by the effect of surface tension on the wire ($\pi D\sigma$) was at a minimum of 7% of the buoyancy force (Δmg) and a maximum of 28% of the buoyancy force across participants, which provided the information necessary to perform this estimate. However, all participants corrected for this effect except for participant 132. Differences in the effectiveness of these corrections cannot be determined with the information provided by participants. However, the fact that participant 132's data are consistent with participant 122 and 172's data,

https://doi.org/10.1021/acs.jced.5c00421
J. Chem. Eng. Data XXXX, XXX, XXX−XXX

Table 10. Values for the Linear Relationships of Density as a Function of Temperature ($\rho = m \times T$ (°C) + b [g cm^{-3}]) from Figures 4 and 5, as well as the Determined Density at 600 °C (FLiNaK) and 700 °C (FLiNaK and NaCl-KCl)

	FLiNaK				NaCl-KCl		
group	m (×10^4)	b	ρ (600 °C)	ρ (700 °C)	m (×10^4)	b	ρ (700 °C)
122	−6.32 ± 0.07	2.412 ± 0.005	2.033	1.970	−5.55 ± 0.09	1.963 ± 0.007	1.575
132	−6.56 ± 0.15	2.43 ± 0.09	2.036	1.971	−5.5 ± 0.3	1.96 ± 0.02	1.575
135	−5.8 ± 1.0	2.43 ± 0.06	2.082	2.024	−5.55 ± 0.07	1.99 ± 0.06	1.602
169	−5.6 ± 0.3	2.34 ± 0.02	2.004	1.948	−5.0 ± 0.6	1.86 ± 0.04	1.510
172	−6.6 ± 1.2	2.45 ± 0.07	2.054	1.988	−5.93 ± 0.16	1.981 ± 0.015	1.566
179	−6.8 ± 1.4	2.49 ± 0.09	2.082	2.014			

which had been corrected, indicates that the effects of any differences in this correction are minor.

Uncertainty in the temperature measurement is likely the major contributor to errors in the density measurements. Table 3 lists reported uncertainty in temperature ranging from ±2 to ±20 °C. Apart from errors introduced by calibration by the thermocouple manufacturers, errors can also be introduced by the placement of thermocouples inside furnaces. In a typical tube furnace, the temperature can vary by tens of degrees depending on the position inside the furnace. The difference in temperatures required to achieve identical density values using the regressed correlations provides an estimate of the possible temperature uncertainty between groups. The regression lines for Groups 135 and 169 indicate that FLiNaK has a density of 2.05 g cm^{-3} at 655 and 517 °C, respectively, representing a 138 °C difference. Similarly, the temperature difference between the two groups is 172 °C at a density of 1.55 g cm^{-3} for the NaCl-KCl eutectic. Further support for the case that temperature is a major contribution to the error is that Group 169 reports a density for the provided NaCl-KCl at 640 °C. However, this temperature is below all measured values of the melting point of this NaCl-KCl salt (Section 3.1.4). This data point was measured on a cooling run, and in principle, the salt could have remained liquid due to supercooling, which has been observed in DSC runs to be as much as 20 °C for halide salts. However, because the bob is raised and lowered through the surface of the salt during this measurement, it is more likely that a temperature difference existed between the thermocouple and salt temperatures, which was not calibrated for in the experimental setup.

Groups 122, 132, 169, and 179 placed the thermocouple directly into the salts, while groups 135 and 172 used a pretest correlation of furnace temperature to in-salt temperature in a placeholder salt to determine appropriate set points. While no groups reported using any shielding materials on the thermocouple, the use of shielding materials can be another source of error in the temperature measurement, introducing differences of tens of degrees between measured and actual temperatures. The drastic differences between the measured density at a single temperature for participants 135 and 169 could be caused by this difference in the thermocouple placement. Thermocouples in salt can become significant heat sinks[37] introducing temperature gradients in the crucible, which may affect density measurements.

Thermal expansivity results are robust despite potential temperature calibration errors, as seen in the insets in Figures 4 and 5. Although Groups 135 and 169 measure statistically different densities for both salts, their thermal expansivity values are not statistically different (excluding the anomalous FLiNaK heating run from Group 169).

Treating the measured density values from all participants as a single data set, a regression fit of $\rho = -6.85 \times 10^{-4}\ T$ (°C) + 2.45 for FLiNaK fits all of the measured data with a maximum residual of only 5%, and a regression fit for the measured density data of NaCl-KCl salt yields $\rho = -5.95 \times 10^{-4}\ T$ (°C) + 1.97, which fits all of the measured data with a maximum residual of again only 5%. This indicates that even with significant variation in the application of a single measurement method, reasonably consistent results can be obtained.

3.1.4. Melting Point. The primary aim of repeated measurements of melting points on FLiNaK and NaCl-KCl systems across different laboratories was to determine and suggest the most appropriate values and identify possible reasons for discrepancies. The aim was not to have all instruments and experimental procedures uniform; thus, different apparatuses and experimental conditions were applied.

Melting point measurements for both salts are shown in Figure 6. The capped error bar on each measurement represents the 95% confidence interval calculated from the standard deviation of replicate measurements, which is represented by the right-hand error arrow with small tips. Where available, self-reported errors appear as the leftmost error arrow with large tips. Self-reported arrows account for systematic errors, such as temperature calibration, that are not improved by repeated measurements, and/or geometry of the tailor-made measurement crucible that can add uncertainty on the final results. Group 124 performed four measurements of each salt at different ramp rates and extrapolated the measurements to the 0 K min^{-1} ramp rate (to yield, in principle, the "thermodynamic temperature"). As all their data are pooled into an extrapolation, the standard deviation of melting points is not reported.

The uncertainty in melting points is dominated by systematic errors. Seven groups (124, 125, 135, 137, 169, 180, and 193) measured the melting points of both salts. For both salts, the melting points reported by the five groups are in the same relative order: 180 > 169 > 124 > 137 > 135. Self-reported errors, where available, were generally larger than the associated standard deviation of measurements and confidence intervals from those groups, except for the case of FLiNaK from Group 169. In some cases, e.g., Groups 137 and 180 for NaCl-KCl eutectic, the previous literature value is included in the self-reported error estimate but not the statistical error estimate.

The nature of the systematic biases is unclear. In principle, faster ramp rates can lead to overestimates of melting points when the temperature is not calibrated because the sample temperature lags behind the temperature in the DSC, and this dependence of onset point and heat rate should be well-characterized.[59] This can partly be accounted for in the

https://doi.org/10.1021/acs.jced.5c00421
J. Chem. Eng. Data XXXX, XXX, XXX−XXX

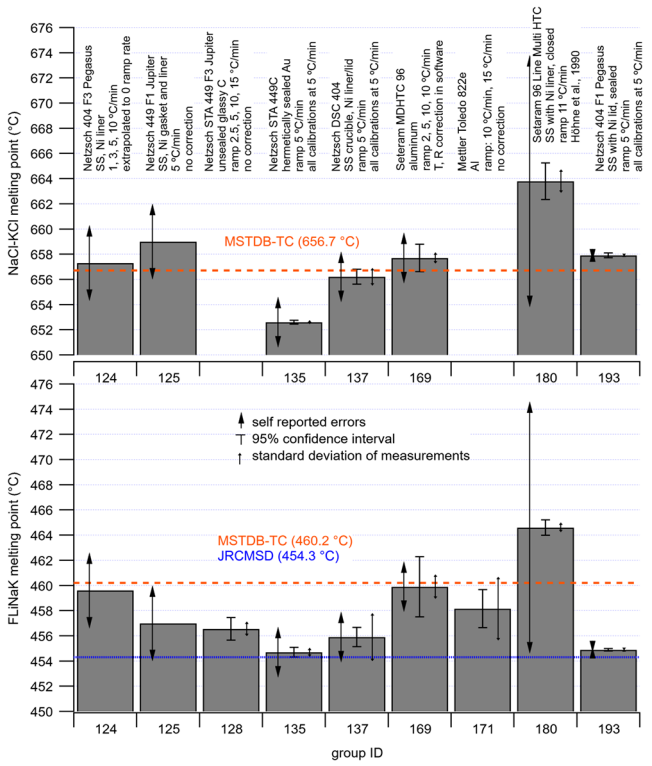

Figure 6. Melting points of NaCl-KCl (top) and FLiNaK (bottom). In both panels, the leftmost error arrows represent self-reported error estimates. Center-capped error bars represent 95% confidence intervals. The right-most error arrows represent the standard deviations of measurements, from which the 95% confidence interval is derived. Labels at the top of the graph are shortened summaries of the measurement approach details, as listed in Table 5. Tabulated values of melting point measurements are reported in Table S-4 in the Supporting Information.

calibration based on the heating rate effects. Extrapolation to 0 K min^{-1} ramp rate, as performed by Group 124, is expected to yield the lowest melting points, but their melting point results are second highest for FLiNaK and the median for NaCl-KCl eutectic. Groups 135, 137, and 193 performed all DSC calibrations and measurements at a ramp rate of 5 °C min^{-1}. Although their measurements for both salts are near the lowest among all groups, the differences are not consistent. For FLiNaK, the melting point measured by Group 137 is more similar to that of Group 135 compared to that of Group 124. However, for the NaCl-KCl eutectic, this relationship is reversed. Group 180 performed measurements at 11 °C min^{-1}, but their melting points are highest for both salts, even though Groups 128 and 171 performed DSC measurements at ramp rates as high as 15 °C min^{-1}. In addition to the method employed for temperature correction, other systematic differences, such as DSC mode, crucible selection, and standards used in calibration, must be explored to understand the causes of these discrepancies. It is worth noting that differences in thermal conductivity and thermal properties between the standards and the samples will impact the applicability/reliability of the temperature correction, with a more pronounced effect at faster heating rates.[60]

In addition, several other factors might lead to minor differences in the heat flow curve shapes, which might influence the identification of the onset (by shifting to lower or higher temperatures). Some groups reported a relatively large range of sample mass (e.g., Group 128:20−50 mg compared to Group 171:4−7.9 mg). If sample mass differs significantly between two different experiments with the same heating rate, it can result in slightly different shapes of the heating curve and, thus, slight differences in identified onsets.

Another important factor is whether the sample was sealed in a tailor-made crucible or simply covered with a lid. It is known that the melt, after melting, has a certain vapor pressure. Even if this vapor pressure is expected to be low, the small sample weight means some evaporation can occur if the corresponding crucible surface is large (although no mass change was reported for the majority of groups). If the vaporization is not congruent, then a small change in the sample composition can be expected. To illustrate this scenario for unsealed samples, vapor pressures for both mixtures were computed at 100 K higher than their melting point using the MSTDB-TC, yielding values of 0.006 Pa at 830 K and 25 Pa at 1030 K for FLiNaK and 50NaCl-50KCl, respectively. As a general guideline, if vapor pressure is superior to a few dozen Pa, mass losses can start being noticed, depending on the target heating temperature and dwell time (both not reported) for temperature stabilization; higher temperature and longer time will lead to more evaporation. Also, the temperature cycling might follow various strategies; the heating−cooling cycling can oscillate from 30 to 50 °C around the melting point, depending on the selected heating rate.

Sample handling to prevent moisture contamination seems to be a difficult problem to control. It is probably impossible to exclude traces of oxygen in the sample. This trace oxygen may be present in a variety of forms—as oxides, oxyhalides, water moisture, or molecular oxygen (due to its presence in Ar gas). All of these forms result in different chemical processes that are connected with the material of the sample holder. The impurities of some metals in FLiNaK, even in parts per million amounts, can also be involved in the corrosion process, which is significantly enhanced if water moisture is present (photos of the container after measurements would be useful to qualitatively confirm or exclude corrosion). Group 135's use of a gold crucible helped reduce corrosion, as previous studies have used gold as a stable quasi-reference electrode because of gold's corrosion resistance in molten salts.[61] Finally, if the sample was not exactly the eutectic composition, small changes in the composition will result in wider signals (i.e., overlapping primary liquidus point and eutectic on the heating ramp, which is not easily detectable).

The average values obtained for both salts, considering all measurements and the self-reported uncertainties, are (657.8 ± 1.5) and (457.9 ± 1.9) °C for the NaCl-KCl and FLiNaK salts, respectively. This can be compared to Janz's and Pelton's compiled and reviewed experimental data,[62,63] and values calculated with the MSTDB and JRCMSD (656.7 °C and 460.2/454.3 °C, respectively, see Figure 2). The agreement with the predictions from the thermodynamic models, considering the uncertainty on the composition (Section 3.1) and the variability of measurement methods, is good. Janz recommended (454 °C) for the FLiNaK salt, based on the review of data collected in the 1940−1960s. It is worth noting that data at that time was often derived from cooling, well-known for problematic undercooling effects. It is also not clear how pure the samples were in those studies, which might explain the different results. The value cited by Pelton[64] for NaCl-KCl, i.e., 658 °C, is in excellent agreement with the data measured here.

https://doi.org/10.1021/acs.jced.5c00421
J. Chem. Eng. Data XXXX, XXX, XXX−XXX

3.1.5. Thermal Conductivity. Thermal conductivity results are listed in Figure 7. Linear regressions (Table 11) are not

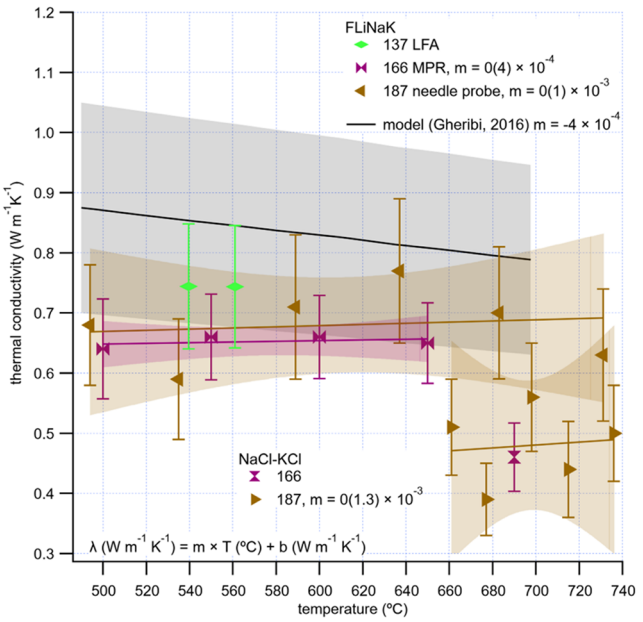

Figure 7. Thermal conductivity of FLiNaK and NaCl-KCl eutectic. For data produced in this work, error bars represent uncertainty propagation calculated by individual groups, and error bands are 95% confidence bands of linear fits. An equilibrium modeling dynamics (EMD) prediction is shown in black with error bands as defined in those works.[9,65,66] Tabulated values of thermal conductivity and thermal diffusivity measurements are reported in Table S-5 in the Supporting Information.

Table 11. Values for the Linear Relationships of Thermal Conductivity as a Function of Temperature ($k = m \times T(°C) + b$ [$W\ m^{-1}\ K^{-1}$]) from Figure 7, as well as the Determined Thermal Conductivity at 700 °C (FLiNaK and NaCl-KCl)

	FLiNaK			NaCl-KCl		
group	m ($\times 10^4$)	b	k (700 °C)	m ($\times 10^4$)	b	k (700 °C)
166	0.6	0.618	0.66			
187	0.985	0.62	0.68895	2.43	0.311	0.4811

calculated where data at only one or two temperatures were reported. Thermal diffusivity measurements by Group 135 are presented in Table S-5 in the Supporting Information and not included in Figure 7 because supporting property values necessary to convert thermal diffusivity to thermal conductivity were not available. Error bars represent the self-reported uncertainty provided by each group, which can include both systematic and random sources of error. Also shown in Figure 7 are results from modeling by equilibrium modeling dynamics (EMD).[65] The shaded regions represent 95% confidence bands on the linear regression.

The measurements from this work are within the error bars of each other, but not always with previous measurements in the literature. This is expected, as the participants of this study measured a common source of salt, and previous measurements did not. Robertson et al.[9] observed that LFA measurements of FLiNaK thermal conductivity exhibit a greater slope than do transient grating spectroscopy measurements. The thermal conductivity results in this work do not support this observation. The slopes observed in the LFA and needle probe data are not different at 95% confidence.

Theoretical modeling predictions and measurements of unary salts[41] have shown a negative slope,[65] in contrast to the positive slopes observed in this and previous work.[9,66] The results from Groups 166 and 187 are both consistent with slightly positive slopes. The relatively large uncertainty of these measurements and the lack of an existing standard method for salt measurements limit the ability of this work to definitively determine the appropriate slope for the thermal conductivity of LiF-NaF-KF salt. However, the measured FLiNaK thermal conductivities by all four participants are consistent within an order of magnitude with previous work.[65]

3.2. Discussion. This section presents recommendations from each subject area on best measurement practices as part of the lessons learned from the round robin study.

Compositional errors (see summary of results in Tables 12 and 13) associated with salt preparation are considered minimal due to the large sizes of the batches in this study. Unfortunately, the target composition (nominal values provided in Table 12) for the FLiNaK is unknown for reasons listed in Sections Sections 2.2.1 and 3.1, and it is believed to be a long-time established 46.5LiF-11.5NaF-42KF mol % eutectic. Figure 8 highlights the MSTDB-TC computed liquidus temperatures for the compositions provided by each group compared to the nominal and preliminary compositions of FLiNaK. Preliminary ICP-MS measurements reported by ORNL indicated a composition of 45.0LiF-13.7NaF-41.3KF mol %, which originally raised a concern about whether the prepared batch is the eutectic or off-eutectic. This value is questionable based on thermal analysis, where a distinct and sharp eutectic peak without a liquidus shoulder was noted by numerous participants in this round robin and is indicative of a eutectic or near eutectic composition.

For the oxygen analysis (summarized in Table 14), both chloride and fluoride salts were shipped together to each participant; however, the analyses were conducted several years apart. This time gap did not appear to impact the chloride salt results, as all groups reported comparable oxygen concentrations within one standard deviation in chloride salt. In contrast, a more pronounced difference was observed in the oxygen concentrations of the fluoride salt. One potential explanation is the variation in the physical form of the salts received: Group 135 received prepowdered salt that required no further processing, while Groups 137 and 200 received solid chunks that were subsequently ground into powder using an agate mortar and pestle inside a glovebox. All three groups encapsulated their samples within glovebox environments. The fact that this discrepancy was only observed in the fluoride salt suggests that transportation alone is unlikely to be the primary source of variation. Rather, it may indicate a compromised vessel integrity for the fluoride salt provided to Group 135, as the received salts were already in a powdered state. However, oxygen measurements of chloride salt were still comparable with other groups, as the measured oxygen values remained within the range of standard deviation, despite being slightly higher. Additional factors, such as sample preparation and storage conditions, may also have contributed to the dissimilarity of results, especially since the salts were transported in their native form without being sealed in analysis capsules. Notably, when sample preparation methods were consistent—as in the case of Groups 137 and 200—oxygen measurements were closely aligned, despite the use of

https://doi.org/10.1021/acs.jced.5c00421
J. Chem. Eng. Data XXXX, XXX, XXX−XXX

Table 12. Summary of Compositional Analysis for FLiNaK Salt (normalized to 100%) Is Listed alongside Measured Melting Points and Computed Values Using MSTDB-TC for the Anticipated Temperature for the Eutectic and Liquidus for the Given Composition

						computed (MSTDB-TC)	
group	instrument	LiF	NaF	KF	measured	eutectic	liquidus
			mol(%)		T (K)	T (K)	T (K)
nominal		46.5	11.5	42		732.9	733.5
preliminary − ORNL	ICP-MS	45.0	13.7	41.3		732.9	762.0
124	ICP-OES	46.4 (4)	11.4 (6)	42.2 (8)	732.8	732.9	735.2
125					730.2	732.9	
128					729.7	732.9	
135	ICP-OES	47.9 (1.3)	11.5 (3)	40.6 (1.4)	727.9	732.9	751.7
137	ICP-OES	46.1 (4)	11.6 (1.0)	42.3 (4)	729.1	732.9	737.8
147	ICP-MS	44.1 (1.3)	12.9 (5)	43 (2)		732.9	754.4
169					733.1	732.9	
171	ICP-MS	44.3 (6)	11.9 (6)	43.8 (1.1)	731.3	732.9	759.8
172	ICP-OES	46.6 (1.8)	11.8 (5)	41.6 (1.8)		732.9	735.6
180					737.8	732.9	
200	ICP-MS	45.4 (0.4)	11.4 (0.1)	43.2 (0.4)		732.9	749.1

Table 13. Summary of Compositional Analysis for the NaCl-KCl Salt

group	instrument	NaCl	KCl
nominal		50	50
135	ICP-OES	50.1 (1.5)	49.9 (7)
147	ICP-MS	50 (4)	50 (7)
172	ICP-OES	50.5 (9)	49.5 (1.0)
200	ICP-MS	48.8 (0.5)	51.2 (0.5)

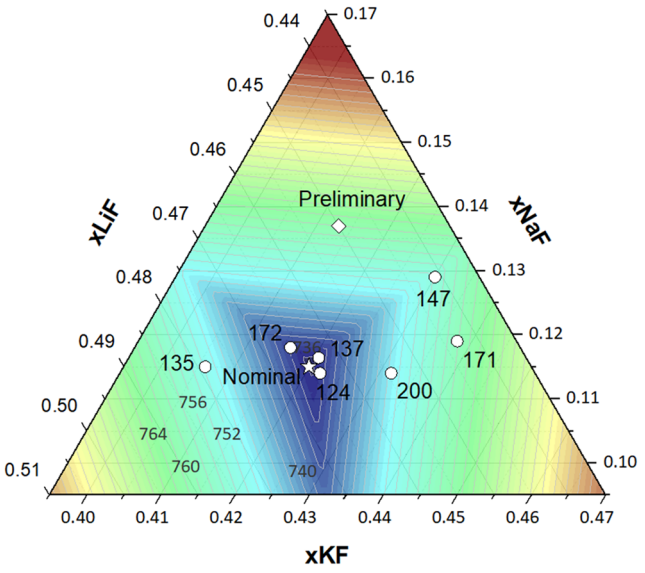

Figure 8. Computed liquidus projection in K near the nominal FLiNaK eutectic using MSTDB-TC together with reported compositions measured in this work by different groups. Each line in the temperature projection represents a change of 2 K.

Table 14. Summary of the Oxygen Analysis

group	FLiNaK (O wppm)	NaCl-KCl (O wppm)
135	1865 (439)	450 (171)
137	489 (16)	208 (47)
200	466 (54)	339 (45)

different IGF analyzers from varying manufacturers and models.

All participants received salts from the same batch, packaged in the same manner. Because of this, the most significant variability would occur once the salts were removed from their packaging and handled in individual laboratories. While oxygen concentration measurements could provide insight into salt hygroscopicity, not all participating laboratories had this capability, preventing a systematic evaluation of its relationship with oxygen uptake and density. Moreover, there were not enough overlapping data between groups performing oxygen analysis and those conducting density measurements to establish a reliable correlation. For these reasons, a discussion of hygroscopic effects was considered outside the scope of this study.

The effects of systematic errors in particular measurements are illustrated by plots showing the correlation of each group's results for NaCl-KCl and FLiNaK. These plots are shown in Figure 9. At 95% confidence, the slope of the melting point correlation plot is statistically compatible with unity, showing that each degree of error in one salt corresponds to one degree of error in the other. This is unsurprising since the melting point is a direct measurement, and thus, it is expected to be sensitive to the absolute temperature calibration of the DSC. In contrast, the slope of the correlation plot of volume expansivities is compatible with zero at 95% confidence, indicating that the error in one salt does not translate to an error in the other. This is even though the densities from which the expansivities are calculated exhibit unambiguous systematic bias explained above. We note that the correlation of the density at 700 °C has a slope compatible with zero at 95% confidence. Given that we have identified sources of systematic error in the density measurements, we caution against assuming that there is no correlation in the data. Therefore, although density is sensitive to errors in absolute calibration, the derived quantity of expansivity remains robust. We recommend that attention be paid to the effect that absolute and relative errors have on the derived quantities; it is possible that a strictly theoretical propagation of error may overstate the uncertainty.

The following paragraph describes several observations about density measurements, namely, the methodology used

https://doi.org/10.1021/acs.jced.5c00421
J. Chem. Eng. Data XXXX, XXX, XXX−XXX

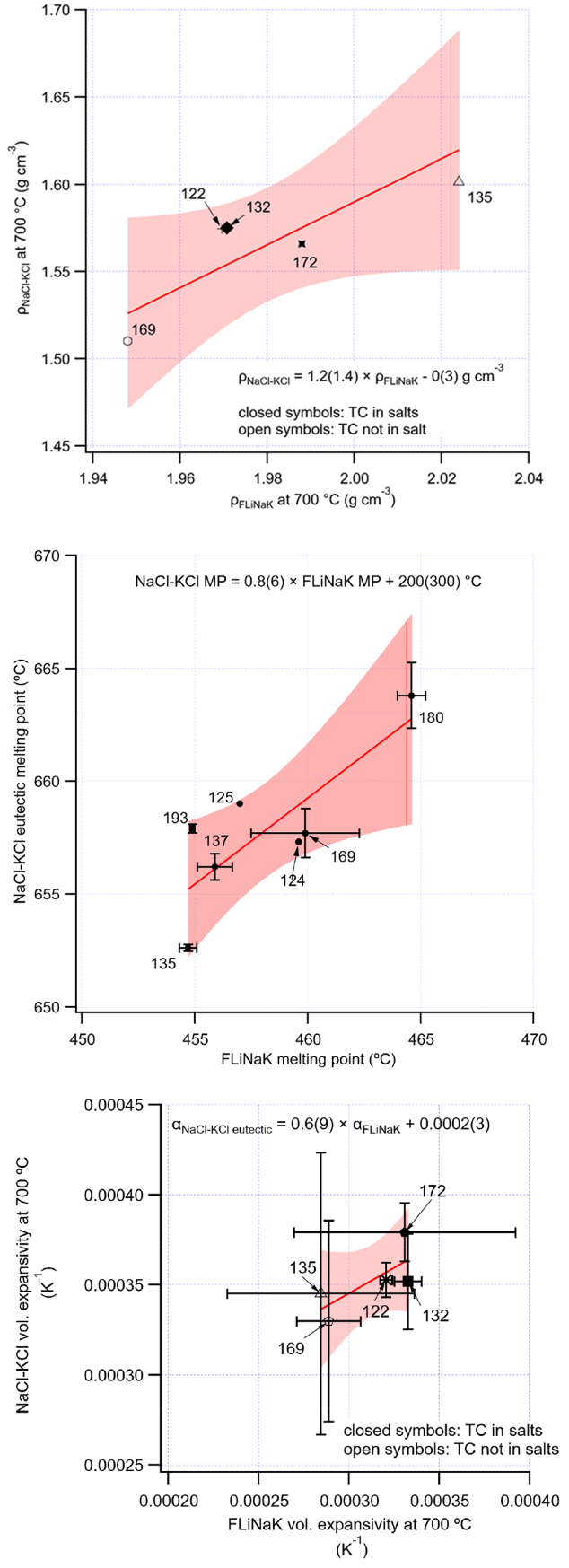

Figure 9. Comparison of the Densities (top), melting points (middle), and expansions (bottom) of both salts.

by groups, error sources, confounding issues, surface tension effects, and the consistency of measured values. Round robin participants independently selected a single method of measuring density, namely, the hydrostatic method based on Archimedes' principle of buoyancy. This method is highly adaptable to molten salts and easy to implement in an oxygen- and moisture-free environment. Temperature calibration is the dominant source of uncertainty in density measurements by the hydrostatic method. To limit parasitic heat losses, one method is to use a pretest calibration of in-salt temperature to furnace setting, rather than a thermocouple in the salt during measurements. Comparisons of measured values were complicated by using different linear thermal expansion values for the same bobber materials in the postprocessing of the data. When publishing new density data, raw data and all of the postprocessing parameters and their uncertainties must be provided, including volume calibration of the bobber at room temperature, mass of the bobber, assumed thermal expansivity of the bobber material, wire diameter, and wire immersion volume. The surface tension effects should be minimized by using a thin wire to prevent the need for correction of surface tension. Despite differences in the temperature calibration, linear thermal expansion values, corrections for surface tension, and materials used, a consistent value for thermal expansivity of the salts was obtained for each salt.

As for melting point measurements, it is important to see that multiple measurements of such a fundamental property resulted in a relatively wide range of melting point values, from 454.7 to 464.6 °C for FLiNaK. Based on the results above, we can provide a few simple general recommendations that would yield the most reliable values for melting point using the DSC method. These recommendations include crucible design, calibration sources, heat rate impact, and potential volatilization issues. One lesson from this round robin about DSC measurements is that the community has not converged on the most suitable crucible design for transition temperature measurements in molten salts. While a stainless steel crucible with a nickel liner is most popular, it is unclear if this is the optimal design. There is value in installing DSC/STA equipment in an inert glovebox. Participants in the round robin test did not use a consistent set of calibrants, even when using the same crucible. Some groups used metals, some used unary salts, and some used mixtures. Key considerations when selecting calibrants include the following: a reasonable assurance of purity (which is hard to do with mixtures), thermal properties that span the range of the materials of interest, standardization of sources, etc. There are inconsistencies in the corrections applied for the effects of heating rates, even when using the same instrument and crucible design. Significant differences in the corrected values might indicate issues with the calibration procedure and/or issues with overlapping thermal events. For a system with eutectic and liquidus transitions close to each other, the two events might be "merged" on heating into one peak, and difficult to distinguish, especially at fast heating rates. Such overlapping events are usually better distinguished on cooling curves. Thus, although we recommend extracting temperatures from the heating curves, the cooling curves are also very informative and should be carefully scrutinized. However, it is unclear what the specific heating rates should be, and if they will be instrument-specific. One potential option could be heating rates of 2.5, 5, and 10 K/min and extrapolating to the 0 K/min value. Ideally, multiple ground samples (each freshly pressed and of

https://doi.org/10.1021/acs.jced.5c00421
J. Chem. Eng. Data XXXX, XXX, XXX−XXX

comparable weight) would be measured at these different heating rates over at least two cycles (heating−dwell−cooling−dwell−heating−dwell−cooling). There are situations that lead to preferential (incongruent) vaporization, whereby post-DSC elemental analyses are prudent to understand any potential changes to composition (e.g., via ICP-MS and/or X-ray diffraction). This has been seen over longer time scales, for example, during viscosity or density measurements that take >4 h to complete. This is not typically observed when using sealed crucibles during DSC measurements, but it may be an issue when using a very slow scan rate in an open crucible with some salt mixtures.

The results shown in Section 3.1.5 demonstrated that different methodologies resulted in similar measurements of the thermal conductivity when considering the uncertainties reported by each group. However, several issues measuring thermal conductivity have been highlighted by this round robin, including the lack of measurement standards, error and uncertainty, and experimental design. The lack of standard reference materials and measurement standards for molten salt thermal conductivity makes it difficult for establishing a standard measurement method for salt properties. Several ASTM, DIN, and ISO standards exist for laser flash analysis when applied to solids, but none for liquids. Several ASTM standards exist for liquid measurements of thermal conductivity, but none are valid in the temperature range for molten salts. Standard reference liquids are limited to toluene and water, which cannot be tested at the temperature ranges experienced by molten salts, although nitrate salts and noble gases have been used as high temperature, quasi-reference liquids. We recommend that new standard methods and materials be established that can be used for halide salts to allow a true interlaboratory study to resolve discrepancies in thermal conductivity measurements. Further, a well-established error analysis, such as that provided by the transient hot wire approach,[53] should be agreed upon. Round robin participants used both direct (fitting for thermal conductivity) and indirect (determining thermal effusivity of diffusivity) methods. Because of this, each measurement of thermal conductivity is dependent in some way on the specific heat and density of the salt, which can impact measurement error through the propagation of uncertainty. Reported measurement uncertainties were 10−17%, which are large enough that the community cannot resolve the issue of the temperature dependence of thermal conductivity (dk/dT). Measurement uncertainties below 5% would help to address this problem. Container design and materials should be designed to limit non-conductive heat transfer along the measured dimensions. This can include limiting the radial heat conduction in LFA crucibles or the axial conduction in needle probe measurements. Additionally, experimental designs should limit or eliminate the convective and radiative heat transfer through the salt.

4. CONCLUSIONS

An international round robin was conducted by seven government laboratories/institutes and 14 universities to study the measurement of salt composition, oxygen content, density, melting point, and thermal conductivity using common batches with target compositions of equimolar eutectic NaCl-KCl and 45.0LiF-13.7NaF-41.3KF mol % (FLiNaK), and the anonymized results are presented here. The objective was to compare measurement results on each of the two consistent batches of salts to establish a baseline for future salt property determinations.

Samples from identical salt batches were provided to multiple laboratories for characterization of composition, transition temperatures, density, and thermal conductivity. This includes details about the experimental methodologies and potential uncertainties in the results. The determination of original NaCl-KCl and FLiNaK sample compositions saw reasonable agreement among all but one of the laboratories. Oxygen analysis was limited to three laboratories with capability, with one reporting significantly larger amounts than the other two. For density measurements, with one exception, all participant data showed a similar trend with temperature and agreed within <0.1 g/cm^3 with a similar level of agreement in expansivity. The melting temperatures for the salt mixtures saw significant agreement among the participants, with four agreeing within 3 °C and all six within 6 °C. Thermal conductivity measurements were provided by three participants for FLiNaK and only two for NaCl-KCl, all exhibiting a significant spread among the individual measurements. In contrast, those obtained from the linear regression for FLiNaK values for two of the participants were within ∼0.2 W m^{-1} K^{-1}, and for NaCl-KCl, the linear regression for the values at multiple temperatures from one participant agreed within that same limit with the single value provided by the second participant. The most replicable property measurements were compositional analysis, density, and melting point, while the least replicable measurements were thermal conductivity and oxygen content. Further, oxygen concentrations of chloride salts were comparable when taking standard deviations into consideration. However, this was not the case for fluoride salts.

The evaluations in this study identified areas for improvement in molten salt thermophysical property quantification, and a series of recommendations were developed. Commercial measurement systems were used for melting point, composition, and oxygen content measurements, while density measurements were performed with in-house developed systems. For thermal conductivity, both commercial systems (laser flash) and in-house-developed systems (modulated photothermal radiometry and needle probe)were used. With respect to the measurement of density, those included the usage of the hydrostatic method using thin wires with standard coefficient of thermal expansion values to reduce the effect of molten salt surface tension, as well as a pretest calibration of in-salt temperature to reduce temperature uncertainty. Analysis of the DSC measurement for melting point led to the conclusion that measurements would benefit from being performed in an inert atmosphere glovebox using standardized crucibles and calibration standards, as well as the use of multiple heating rates to obtain heating rate correction. Review of the thermal conductivity studies revealed a general lack of the existence of standard reference liquids for high temperature validation, as well as the need for container designs and materials that reduce radiative and convective heat transfer in the salt and container. Also, due to the dependence of the calculation of thermal conductivity on other experimental variables, the propagation of errors from the determination of those variables can lead to a high level of uncertainty in the reported thermal conductivity. These results, along with guidance based on the details of the measurements described above, on the various sample handling, measurement, and evaluation of property value methodologies, will contribute to the ongoing efforts to

https://doi.org/10.1021/acs.jced.5c00421
J. Chem. Eng. Data XXXX, XXX, XXX−XXX

provide standardized, best practice approaches to salt characterization for nuclear applications.

■ ASSOCIATED CONTENT

Supporting Information

The Supporting Information is available free of charge at https://pubs.acs.org/doi/10.1021/acs.jced.5c00421.

Data files, method description for each group, and round robin participant forms (ZIP)

Literature values of FLiNaK's melting point and density, and tabulated summary of density, melting point, thermal conductivity, and thermal diffusivity measured data with uncertainty (PDF)

■ AUTHOR INFORMATION

Corresponding Author

Raluca O. Scarlat − *University of California, Berkeley, Berkeley, California 94720, United States;* orcid.org/0000-0003-3302-1142; Email: scarlat@berkeley.edu

Authors

Troy Munro − *Brigham Young University, Provo, Utah 84602, United States;* orcid.org/0000-0002-2557-4911

Randall Chiu − *University of California, Berkeley, Berkeley, California 94720, United States*

Melissa A. Rose − *Argonne National Laboratory, Lemont, Illinois 60439, United States*

Ondrej Benes − *European Commission, Joint Research Centre, Karlsruhe NUTS DE122, Germany*

Miroslav Boca − *Slovak Academy of Sciences, Bratislava 84536, Slovakia*

D. Nathanael Gardner − *University of California, Berkeley, Berkeley, California 94720, United States;* orcid.org/0000-0001-8780-6004

Amanda Leong − *Virginia Polytechnic Institute and State University, Blacksburg, Virginia 24061, United States*

Sara Mastromarino − *University of California, Berkeley, Berkeley, California 94720, United States*

Kim L. Pamplin − *Abilene Christian University, Abilene, Texas 79699, United States*

Markus H. A. Piro − *McMaster University, Hamilton, ON L8S 4L7, Canada*

Mouna Saoudi − *Canadian Nuclear Laboratories, Chalk River, ON K0J 1J0, Canada*

Juliano Schorne-Pinto − *University of South Carolina, Columbia, South Carolina 29208, United States;* orcid.org/0000-0003-4208-4815

Christian Michael Sclafani − *University of California, Berkeley, Berkeley, California 94720, United States;* orcid.org/0000-0002-1982-8305

Anna L. Smith − *Delft University of Technology, Radiation Science and Technology department, Delft 2629 JB, Netherlands;* orcid.org/0000-0002-0355-5859

Nathan D. Smith − *Pennsylvania State University, Materials Science and Engineering, University Park, Pennsylvania 16802, United States*

Dino Sulejmanovic − *Oak Ridge National Laboratory, Enrichment Science and Engineering Division, Oak Ridge, Tennessee 37831, United States;* orcid.org/0000-0002-4165-724X

Allison M. Berry − *Abilene Christian University, Abilene, Texas 79699, United States*

Renkun Chen − *University of California, San Diego, La Jolla, California 92093, United States;* orcid.org/0000-0001-7526-4981

Ka Man Chung − *University of California, San Diego, La Jolla, California 92093, United States*

Christa Dahman − *Wisconsin State Laboratory of Hygiene, Trace Element Clean Lab, Madison, Wisconsin 53706, United States;* orcid.org/0009-0000-4572-0835

Kent Detrick − *Brigham Young University, Provo, Utah 84602, United States*

Tianshi Feng − *University of California, San Diego, La Jolla, California 92093, United States*

J. A. Ocádiz Flores − *Delft University of Technology, Radiation Science and Technology department, Delft 2629 JB, Netherlands*

Ryan Gallagher − *Oak Ridge National Laboratory, Enrichment Science and Engineering Division, Oak Ridge, Tennessee 37831, United States; Ohio State University, Department of Nuclear Engineering, Columbus, Ohio 43210, United States;* orcid.org/0000-0002-5372-6644

Levi Gardner − *Argonne National Laboratory, Lemont, Illinois 60439, United States*

Xiaofeng Guo − *Washington State University, Pullman, Washington 99163, United States;* orcid.org/0000-0003-3129-493X

J. Matthew Jackson − *Los Alamos National Laboratory, Los Alamos, New Mexico 87545, United States*

Toni Karlsson − *Idaho National Laboratory, Idaho Falls, Idaho 83415, United States*

Peter Kasper − *Brigham Young University, Provo, Utah 84602, United States*

Hojong Kim − *Pennsylvania State University, Materials Science and Engineering, University Park, Pennsylvania 16802, United States;* orcid.org/0000-0002-6247-3474

Logan McIlwain − *Virginia Polytechnic Institute and State University, Blacksburg, Virginia 24061, United States;* orcid.org/0009-0000-6807-520X

Matthew Memmott − *Brigham Young University, Provo, Utah 84602, United States*

Brian Merritt − *Brigham Young University, Provo, Utah 84602, United States;* orcid.org/0000-0001-8948-2605

Marisa J. Monreal − *Los Alamos National Laboratory, Los Alamos, New Mexico 87545, United States*

Kentaro Oishi − *Polytechnique Montréal, Montréal, Québec H3C 3A7, Canada*

Liana Orlovskaya − *Canadian Nuclear Laboratories, Chalk River, ON K0J 1J0, Canada*

S. Scott Parker − *Los Alamos National Laboratory, Los Alamos, New Mexico 87545, United States*

Andrew A. Prudil − *Canadian Nuclear Laboratories, Chalk River, ON K0J 1J0, Canada;* orcid.org/0000-0001-7455-1620

Aaron D. Robison − *Abilene Christian University, Abilene, Texas 79699, United States*

Sean Scott − *Wisconsin State Laboratory of Hygiene, Trace Element Clean Lab, Madison, Wisconsin 53706, United States*

Raul C. Romero, III − *Abilene Christian University, Abilene, Texas 79699, United States*

John Vlieland − *Delft University of Technology, Radiation Science and Technology department, Delft 2629 JB, Netherlands*

Michael E. Woods − *Idaho National Laboratory, Idaho Falls, Idaho 83415, United States;* orcid.org/0000-0001-8685-6026

Jinsuo Zhang − *Virginia Polytechnic Institute and State University, Blacksburg, Virginia 24061, United States*

Theodore M. Besmann − *University of South Carolina, Columbia, South Carolina 29208, United States*

Complete contact information is available at: https://pubs.acs.org/10.1021/acs.jced.5c00421

Author Contributions

A.D.R.: Investigation. A.M.B.: Methodology, formal analysis, and investigation. A.L.: Formal analysis, investigation, and writing. A.A.P.: Methodology, software, and formal analysis. A.L.S.: Formal analysis, writing—review and editing, and supervision. B.M.: Methodology, software, and investigation. C.D.: Investigation. C.M.S.: Conceptualization, investigation, resources, writing—review and editing, visualization, and project administration. D.N.G.: Methodology, formal analysis, investigation, and writing—review and editing. D.S.: Investigation. H.K.: Validation, data curation, and writing—review and editing. J.M.J.: Methodology, resources, and supervision. J.A.O.F.: Investigation. J.Z.: Conceptualization. J.V.: Investigation. J.S.-P.: Investigation, writing—review and editing. K.M.C.: Methodology and investigation. K.D.: Methodology, validation, formal analysis, investigation, and resources. K.O.: Validation. K.L.P.: Methodology, validation, formal analysis, resources, and writing—review and Editing. L.O.: Validation and investigation. L.G.: Formal analysis, investigation, and writing—review and Editing. L.M.: Investigation. M.J.M.: Writing—review and editing, project administration, and funding acquisition. M.H.A.P.: Analysis and review. M.M.: Conceptualization, methodology, and writing—review and Editing. M.A.R.: Methodology, validation, investigation, data curation, writing—original draft, and writing—review and Editing. M.E.W.: Validation, investigation, and writing—review and editing. M.B.: Writing—review. M.S.: Methodology, validation, formal analysis, and writing—review and editing, Project administration. N.D.S.: Methodology, investigation, and writing—Review and editing. O.B.: Formal analysis, investigation, writing—review and editing. P.K.: Investigation. R.O.S.: Conceptualization, writing—review and editing, supervision, project administration, and funding acquisition. R.C.: Writing—original draft, writing—review and editing, methodology, and project administration. R.C.R.: Methodology, formal analysis and investigation. R.C.: Methodology, resources, writing—review and editing, supervision, and funding acquisition. R.G.: Investigation. S.S.P.: Methodology, validation, formal analysis, and investigation. S.M.: Conceptualization, investigation, resources, data curation, and project administration. S.R.S.: Methodology, investigation and data Curation. T.M.B.: Conceptualization, writing—Review and editing, supervision, project administration, and funding acquisition. T.F.: Investigation. T.K.: Validation, investigation, and funding acquisition. T.M.: Writing—original draft, writing—review and editing, methodology, funding acquisition, and project administration. X.G.: Writing—review and Editing.

Notes

The authors declare the following competing financial interest(s): Over the duration over which the research reported in this manuscript was performed, Scarlat, D. N. Gardner, Zhang, Robison, Romero, Parker, and Memmott had interests in or relationships with entities that are commercializing molten salt technology; the content of this manuscript or the direction of the research presented herein was not influenced by these entities, nor by the authors relationships with these entities. During the time of his involvement, Gallagher was affiliated with Ohio State University and Oak Ridge National Laboratory. He now is employed by Kairos Power LLC, which is not affiliated with this work but is pursuing the commercialization of molten salt reactor technologies. All other authors declare that they have no known competing financial interests or personal relationships that could have appeared to influence the work reported in this paper.

■ ACKNOWLEDGMENTS

This research was performed using funding received from the U.S. Department of Energy (DOE) Office of Nuclear Energy's Nuclear Energy University Program (NEUP): IRP-17-14541, IRP-22-28329, DE-SC0016574, DE-NE0008945, DE-NE19-17413, DE-NE21-24563, DE-NE19-17413 (CID: DENE0008870), DE-NE0009288; US DOE Solar Energy Technologies Office (SETO) Grant No. DE-EE0008379. Graduate students on this project were also supported by the Department of Energy's University Nuclear Leadership Program (DOE-UNLP) and the National Science Foundation Graduate Research Fellowship Program (NSF-GRFP) fellowships. This work was also supported through the INL Laboratory Directed Research & Development (LDRD) Program under DOE Idaho Operations Office Contract DE-AC07-05ID14517. ORNL Subcontract; DOE NE ART MSR Campaign; Laboratory Directed Research and Development (LDRD) program of Los Alamos National Laboratory (LANL) Project No. 20210113DR; DOE-NE Molten Salt Reactor Campaign; Argonne National Laboratory as a U.S. Department of Energy Office of Science laboratory operated by UChicago Argonne, LLC under Contract No. DE-AC02-06CH11357; U.S. Department of Energy Office of Nuclear Energy's Nuclear Energy Advanced Modeling and Simulation Program and the DOE-NE Molten Salt Reactor Program (for the MSTDB-TC development effort), both administered by the Oak Ridge National Laboratory, operated by UT-Battelle, L.L.C., for the U.S. Department of Energy. Additional funding was received by Natura Resources SOW-001; Nuclear Regulatory Commission Award #31310019M0006. Finally, this work was supported by Atomic Energy of Canada Limited's Federal Nuclear Science & Technology Work Plan, Canada Research Chairs program of the Natural Sciences and Engineering Research Council of Canada, grant No. 950-231328, Canadian Nuclear Laboratories grant FST-51120-A120. Funding for equipment from the Canadian Foundation for Innovation, grant No. 35712, the Ontario Ministry of Economic Development, Job Creation Trade, grant No. 35712, and Ontario Power Generation, through the Ontario Tech University Research Infrastructure Fund is greatly acknowledged. The authors would like to acknowledge support by the VT Nuclear Materials Fuel Cycle Center, UW- Wisconsin State Laboratory of Hygiene, the UC Berkeley SALT Laboratory researchers; Matthew Topham for his assistance in data collection; Joel Overdier; Yifen Tsai, Kristin DeAngeles, Susan Lopykinski, and Dr. Seema Naik (ANL Analytical Chemistry Laboratory); Ethan Polselli for density data collection; and Dr. Max Poschmann for melting point measurements.

REFERENCES

(1) Williams, D. F.; Toth, L. M.; Clarno, K. T. *Assessment of Candidate Molten Salt Coolants for the Advanced High-Temperature Reactor (AHTR); ORNL/TM-2006/12*; Oak Ridge National Laboratory, 2006.

(2) Roper, R.; Harkema, M.; Sabharwall, P.; Riddle, C.; Chisholm, B.; Day, B.; Marotta, P. Molten Salt for Advanced Energy Applications: A Review. *Ann. Nucl. Energy* **2022**, *169*, No. 108924.

(3) Faure, B.; Kooyman, T. A Comparison of Actinide Halides for Use in Molten Salt Reactor Fuels. *Prog. Nucl. Energy* **2022**, *144*, No. 104082.

(4) Termini, N.; Birri, T.; Henderson, S.; Ezell, N. D. *An Overview of the Molten Salt Thermal Properties Database− Thermophysical, Version 2.1.1 (MSTDB-TP v.2.1.1); ORNL/TM-2023/2955*; Oak Ridge National Laboratory (ORNL): Oak Ridge, TN (United States), 2023 DOI: 10.2172/1988348.

(5) Besmann, T. M.; Schorne-Pinto, J. Developing Practical Models of Complex Salts for Molten Salt Reactors. *Thermo* **2021**, *1* (2), 168−178.

(6) Beneš, O. Thermodynamic Database on Molten Salt Reactor Systems *Technical report, European Commission*, Joint Research Centre 2021.

(7) Piro, M.; Bajpai, P.; Poschmann, M. *Development of a Gibbs Energy Minimiser for the MOOSE-Based Corrosion Modelling App Yellowjacket and Validation of MSTDB; INL/RPT-22−69782-Rev000*; Idaho National Laboratory (INL), Idaho Falls, ID (United States), 2022. DOI: 10.2172/1963894.

(8) Magnusson, J.; Memmott, M.; Munro, T. Review of Thermophysical Property Methods Applied to Fueled and Un-Fueled Molten Salts. *Ann. Nucl. Energy* **2020**, *146*, No. 107608.

(9) Robertson, S. G.; Wiser, R.; Yang, W.; Kang, D.; Choi, S.; Baglietto, E.; Short, M. P. The Curious Temperature Dependence of Fluoride Molten Salt Thermal Conductivity. *J. Appl. Phys.* **2022**, *131* (22), No. 225102.

(10) Birri, T.; Gallagher, R. C.; Russell, N.; Termini, N.; Rose, P., Jr; Ezell, N. D. *FY22 Progress Report on Viscosity and Thermal Conductivity Measurements of Molten Salts; ORNL/TM-2022/2573*; Oak Ridge National Lab. (ORNL): Oak Ridge, TN (United States), 2022 DOI: 10.2172/1887678.

(11) Ruth, R.; Merritt, B.; Munro, T. Use of a Needle Probe to Measure the Thermal Conductivity of Electrically Conductive Liquids at High Temperatures. *Int. J. Thermophys* **2024**, *45* (11), No. 158.

(12) Schorne-Pinto, J.; Aziziha, M.; Tisdale, H. B.; Mofrad, A. M.; Birri, A.; Christian, M. S.; Ard, J. C.; Booth, R. E.; Yingling, J. A.; Soldan Palma, J. P.; Dixon, C.; zur Loye, H.-C.; Besmann, T. M. Thermal Property Modeling and Assessment of the Physical Properties of FLiNaK. *ACS Appl. Energy Mater.* **2024**, *7*, 4016−4029, DOI: 10.1021/acsaem.4c00321.

(13) Fujisawa, T.; Utigard, T.; Toguri, J. M. Surface Tension and Density of the Molten PbCl2-KCl-NaCl Ternary System. *Can. J. Chem.* **1985**, *63* (5), 1132−1138.

(14) Gutierrez, A.; Toguri, J. M. Densities and Molar Volumes of the Lead(II) Chloride-Potassium Chloride-Sodium Chloride and Lead-(II) Chloride-Potassium Chloride-Lithium Chloride Ternary Systems. *J. Chem. Eng. Data* **1982**, *27* (2), 109−113.

(15) Špet'uch, V.; Petrík, J.; Grambálová, E. The Study of Some Physico-Chemical Properties of Melt KCl-NaCl Mixture. *Metall. Mater. Eng.* **2013**, *19* (1), 23−32.

(16) Van Artsdalen, E. R.; Yaffe, I. S. Electrical Conductance and Density of Molten Salt Systems: KCl−LiCl, KCl−NaCl and KCl−KI. *J. Phys. Chem. A* **1955**, *59* (2), 118−127.

(17) Kunugi, M.; Yamate, T.; Takeuchi, S. Densities of Halide Melts and Molten Glasses in Binary Systems. *J. Japan Soc. Test. Mater.* **1960**, *9* (82), 486−490.

(18) Janz, G. J.; Tomkins, R. P. T.; Allen, C. B.; Downey, J. R.; Garner, G. L.; Krebs, U.; Singer, S. K. Molten Salts: Volume 4, Part 2, Chlorides and Mixtures—Electrical Conductance, Density, Viscosity, and Surface Tension Data. *J. Phys. Chem. Ref. Data* **1975**, *4* (4), 871−1178.

(19) Holm, J. L.; Kullberg, L.; Roti, I.; Okinaka, H.; Kosuge, K.; Kachi, S. Excess Volumes of Mixing in Liquid Binary Alkali Halide Mixtures. *Acta Chem. Scand.* **1971**, *25*, 3609−3615.

(20) Roy, R. R.; Ye, J.; Sahai, Y. Viscosity and Density of Molten Salts Based on Equimolar NaCl-KCl. *Mater. Trans., JIM* **1997**, *38* (6), 566−570.

(21) Katyshev, S.; Dubinin, B.; Desyatnik, V.; Trifonov, K. Density and Surface Tension of Fused Chloride System NaCl-KCl-UCl_4 *Rasplavy* 1998, 4, pp 77−81.

(22) Mayes, R. T.; Kurley, J. M., III; Halstenberg, P. W.; McAlister, A.; Sulejmanovic, D.; Raiman, S. S.; Dai, S.; Pint, B. A. *Purification of Chloride Salts for Concentrated Solar Applications; ORNL/LTR-2018/1052*; Oak Ridge National Laboratory (ORNL): Oak Ridge, TN (United States), 2018 DOI: 10.2172/1506795.

(23) Shaffer, J. H. *Preparation and Handling of Salt Mixtures for the Molten Salt Reactor Experiment; ORNL-4616*; Oak Ridge National Lab. (ORNL): Oak Ridge, TN (United States), 1971 DOI: 10.2172/4074869.

(24) Zong, G.; Zhang, Z.-B.; Sun, J.-H.; Xiao, J.-C. Preparation of High-Purity Molten FLiNaK Salt by the Hydrofluorination Process. *J. Fluorine Chem.* **2017**, *197*, 134−141.

(25) Sulejmanovic, D.; Kurley, J. M.; Robb, K.; Raiman, S. Validating Modern Methods for Impurity Analysis in Fluoride Salts. *J. Nucl. Mater.* **2021**, *553*, No. 152972.

(26) Raiman, S. S.; Kurley, J. M.; Sulejmanovic, D.; Willoughby, A.; Nelson, S.; Mao, K.; Parish, C. M.; Greenwood, M. S.; Pint, B. A. Corrosion of 316H Stainless Steel in Flowing FLiNaK Salt. *J. Nucl. Mater.* **2022**, *561*, No. 153551.

(27) ASTM E691−21. *Standard Practice for Conducting an Interlaboratory Study to Determine the Precision of a Test Method; Standard*; ASTM: West Conshohocken, PA, United States, 2021.

(28) Condon, N. J.; Lopykinski, S.; Carotti, F.; Johnson, T. J.; Kruizenga, A. Method for the Determination of Oxygen in FLiBe via Inert Gas Fusion. *ACS Omega* **2023**, *8* (32), 29789−29793.

(29) Park, J.; Leong, A.; Zhang, J. Static Corrosion of Stainless Steel 316H in Chemically Purified Molten NaF-KF-UF4 Salt. *npj Mater. Degrad.* **2024**, *8* (1), 1−10.

(30) Mohandas, K.; Sanil, N.; Shakila, L.; Vishnu, D. S. M.; Nagarajan, K.Studies on the Electrochemical Deoxidation of Uranium Dioxide in Molten Calcium Chloride *Molten Salts & Ionic Liquids* 2011; Vol. *3*, p 239.

(31) Hughes, S. W. Measuring Liquid Density Using Archimedes' Principle. *Phys. Educ.* **2006**, *41* (5), No. 445.

(32) Touloukian, Y. S.; Kirby, R.; Taylor, R.; Desai, P. *Thermophysical Properties of Matter, the TPRC Data Series: Thermal Expansion - Metallic Elements and Alloys*; IFI-Plenum, 1970; Vol. *12*.

(33) Special Metals. Nickel 200 & 201 Fact Sheet 2006 https://www.specialmetals.com/documents/technical-bulletins/nickel-200.pdf, p. 20. (accessed April 10, 2025).

(34) Callister, W. D., Jr; Rethwisch, D. G. *Materials Science and Engineering: An Introduction*, 7th ed.; John Wiley & Sons, 2007.

(35) Kirby, R. K. Platinum—A Thermal Expansion Reference Material. *Int. J. Thermophys* **1991**, *12* (4), 679−685.

(36) Janz, G. J.; Gardner, G. L.; Krebs, U.; Tomkins, R. P. T. Molten Salts: Volume 4, Part 1, Fluorides and Mixtures Electrical Conductance, Density, Viscosity, and Surface Tension Data. *J. Phys. Chem. Ref. Data* **1974**, *3* (1), 1−115.

(37) Zabirov, A. R.; Molotova, I. A.; Belyaev, I. A.; Ryazantsev, V. A.; Yagov, V. V. Concerning the Methods of Thermocouple Embedding in Experimental Studies of Cooling the High-Temperature Bodies in Subcooled and Saturated Liquids. *Thermophys. Aeromech.* **2021**, *28* (3), 447−454.

(38) Piro, M. H. A.; Lipkina, K.; Hallatt, D. Exploring Crucible Designs for Differential Scanning Calorimetry Measurements of Fluoride Salts. *Thermochim. Acta* **2021**, *699*, No. 178860.

(39) Beneš, O.; Konings, R. J. M.; Wurzer, S.; Sierig, M.; Dockendorf, A. A DSC Study of the NaNO3−KNO3 System Using an Innovative Encapsulation Technique. *Thermochim. Acta* **2010**, *509* (1), 62−66.

https://doi.org/10.1021/acs.jced.5c00421
J. Chem. Eng. Data XXXX, XXX, XXX−XXX

(40) Blumm, J. The Laser Flash Technique: A Widespread Technology for Measurement of the Thermal Diffusivity of Solids and Liquids. *Int. J. Thermophys* **2025**, *46* (3), No. 39.
(41) Chliatzou, Ch. D.; Assael, M. J.; Antoniadis, K. D.; Huber, M. L.; Wakeham, W. A. Reference Correlations for the Thermal Conductivity of 13 Inorganic Molten Salts. *J. Phys. Chem. Ref. Data* **2018**, *47* (3), No. 033104.
(42) Chung, K. M.; Feng, T.; Zeng, J.; Adapa, S. R.; Zhang, X.; Zhao, A. Z.; Zhang, Y.; Li, P.; Zhao, Y.; Garay, J. E.; Chen, R. Thermal Conductivity Measurement Using Modulated Photothermal Radiometry for Nitrate and Chloride Molten Salts. *Int. J. Heat Mass Transfer* **2023**, *217*, No. 124652.
(43) Ramires, M. L. V.; Nieto De Castro, C. A.; Nagasaka, Y.; Nagashima, A.; Assael, M. J.; Wakeham, W. A. Standard Reference Data for the Thermal Conductivity of Water. *J. Phys. Chem. Ref. Data* **1995**, *24* (3), 1377−1381.
(44) Merritt, B.; Seneca, M.; Larson, S.; Davis, K.; Munro, T. Measurements of the Thermal Conductivity of Reference Liquids Using a Modified Transient Hot-Wire Needle Probe. *Int. J. Heat Mass Transfer* **2022**, *189*, No. 122674.
(45) Zhao, A. Z.; Wingert, M. C.; Garay, J. E. Frequency-Domain Hot-Wire Measurements of Molten Nitrate Salt Thermal Conductivity. *J. Chem. Eng. Data* **2021**, *66*, No. 262.
(46) Parker, W. J.; Jenkins, R.; Butler, C.; Abbott, G. Flash Method of Determining Thermal Diffusivity, Heat Capacity, and Thermal Conductivity. *J. Appl. Phys.* **1961**, *32* (9), 1679−1684.
(47) Peng, W.; Wilson, R. B. Nanoscale Laser Flash Measurements of Diffuson Transport in Amorphous Ge and Si. *APL Mater.* **2022**, *10* (4), No. 041111.
(48) Xu, X.; Wang, X.; Li, P.; Li, Y.; Hao, Q.; Xiao, B.; Elsentriecy, H.; Gervasio, D. Experimental Test of Properties of KCl−MgCl2 Eutectic Molten Salt for Heat Transfer and Thermal Storage Fluid in Concentrated Solar Power Systems. *J. Sol. Energy Eng.* **2018**, *140* (5), No. 051011, DOI: 10.1115/1.4040065.
(49) Rudenko, A.; Redkin, A.; Il'ina, E.; Pershina, S.; Mushnikov, P.; Zaikov, Y.; Kumkov, S.; Liu, Y.; Shi, W. Thermal Conductivity of FLiNaK in a Molten State. *Materials* **2022**, *15* (16), No. 5603.
(50) Zhao, A. Z.; Garay, J. E. High Temperature Liquid Thermal Conductivity: A Review of Measurement Techniques, Theoretical Understanding, and Energy Applications. *Prog. Mater. Sci.* **2023**, *139*, No. 101180.
(51) Zeng, J.; Chung, K. M.; Wang, Q.; Wang, X.; Pei, Y.; Li, P.; Chen, R. Measurement of High-Temperature Thermophysical Properties of Bulk and Coatings Using Modulated Photothermal Radiometry. *Int. J. Heat Mass Transfer* **2021**, *170*, No. 120989.
(52) Tian, Z.; Marconnet, A.; Chen, G. Enhancing Solid-Liquid Interface Thermal Transport Using Self-Assembled Monolayers. *Appl. Phys. Lett.* **2015**, *106* (21), No. 211602.
(53) Assael, M. J.; Antoniadis, K. D.; Velliadou, D.; Wakeham, W. A. Correct Use of the Transient Hot-Wire Technique for Thermal Conductivity Measurements on Fluids. *Int. J. Thermophys* **2023**, *44* (6), No. 85.
(54) Bovesecchi, G.; Coppa, P.; Pistacchio, S. A New Thermal Conductivity Probe for High Temperature Tests for the Characterization of Molten Salts. *Rev. Sci. Instrum.* **2018**, *89* (5), No. 055107.
(55) Hollar, C.; Fleming, A.; Davis, K.; Budwig, R.; Jensen, C.; Estrada, D. A Parametric Study for In-Pile Use of the Thermal Conductivity Needle Probe Using a Transient, Multilayered Analytical Model. *Int. J. Therm. Sci.* **2019**, *145*, No. 106028.
(56) Wada, K.; Bateman, A.; Varghese, T. V.; Fleming, A.; Jaques, B. J.; Estrada, D. High Temperature Validation of a Line Heat Source Technique for In-Pile Thermal Conductivity Determination. *Int. J. Therm. Sci.* **2024**, *199*, No. 108907.
(57) Merritt, B.; Seneca, M.; Wright, B.; Cahill, N.; Petersen, N.; Fleming, A.; Munro, T. Thermal Conductivity Characterization of Fluoride and Chloride Molten Salts Using a Modified Transient Hot-Wire Needle Probe. *Int. J. Thermophys* **2022**, *43* (10), No. 149.
(58) Sergeev, D.; Kobertz, D.; Müller, M. Thermodynamics of the NaCl−KCl System. *Thermochim. Acta* **2015**, *606*, 25−33.
(59) Toda, A. Heating Rate Dependence of Melting Peak Temperature Examined by DSC of Heat Flux Type. *J. Therm. Anal. Calorim.* **2016**, *123* (3), 1795−1808.
(60) Höhne, G. W. H.; Hemminger, W.; Flammersheim, H.-J. *Differential Scanning Calorimetry*; Springer, 2003; Vol. 2.
(61) Zhang, J.; Forsberg, C. W.; Simpson, M. F.; Guo, S.; Lam, S. T.; Scarlat, R. O.; Carotti, F.; Chan, K. J.; Singh, P. M.; Doniger, W.; Sridharan, K.; Keiser, J. R. Redox Potential Control in Molten Salt Systems for Corrosion Mitigation. *Corros. Sci.* **2018**, *144*, 44−53.
(62) Sangster, J.; Pelton, A. D. Phase Diagrams and Thermodynamic Properties of the 70 Binary Alkali Halide Systems Having Common Ions. *J. Phys. Chem. Ref. Data* **1987**, *16* (3), 509−561.
(63) Janz, G. J.; Tomkins, R. Physical Properties Data Compilations Relevant to Energy Storage. IV. Molton Salts: Data on Additional Single and Multi-Component Salt Systems; National Standad Reference Data System. 1981.
(64) Pelton, A. D.; Gabriel, A.; Sangster, J. Liquidus Measurements and Coupled Thermodynamic−Phase-Diagram Analysis of the NaCl−KCl System. *J. Chem. Soc., Faraday Trans. 1* **1985**, *81* (5), 1167−1172.
(65) Gheribi, A. E.; Chartrand, P. Thermal Conductivity of Molten Salt Mixtures: Theoretical Model Supported by Equilibrium Molecular Dynamics Simulations. *J. Chem. Phys.* **2016**, *144* (8), No. 084506.
(66) An, X.-H.; Cheng, J.-H.; Yin, H.-Q.; Xie, L.-D.; Zhang, P. Thermal Conductivity of High Temperature Fluoride Molten Salt Determined by Laser Flash Technique. *Int. J. Heat Mass Transfer* **2015**, *90*, 872−877.

https://doi.org/10.1021/acs.jced.5c00421
J. Chem. Eng. Data XXXX, XXX, XXX−XXX